Phytomedicine 123 (2024) 155189

Contents lists available at ScienceDirect

Phytomedicine

journal homepage: www.elsevier.com/locate/phymed

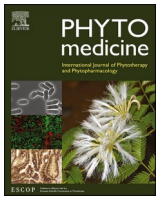

Original Article

Huaier improves the efficacy of anti-PD-L1 Ab in the treatment of hepatocellular carcinoma by regulating tumor immune microenvironment

Huawei Li [a,b,1], Jia You [a,1], Yuanfeng Wei [a], Lingnan Zheng [a], Ju Yang [c], Jingyi Xu [c], Yue Li [c], Zhaojun Li [d], Xi Yang [a,*], Cheng Yi [a,*]

[a] Department of Medical Oncology, Cancer Center, West China Hospital, Sichuan University, Chengdu 610041, China
[b] Department of Integrated Traditional Chinese and Western Medicine, Cancer Hospital, School of Medicine, University of Electronic Science and Technology of China, Chengdu 610041, China
[c] West China School of Basic Medical Science and Forensic Medicine, Sichuan University, Chengdu 610041, China
[d] Department of Radiation Oncology, Hainan General Hospital, Haikou 570311, China

ARTICLE INFO

Keywords:
Huaier
$CD8^+$ T cells
VEGFA
MVD
PD-L1
Anti-PD-L1 Ab

ABSTRACT

Background: Combination therapy is an effective method for augmenting the efficacy of immune checkpoint inhibitors (ICIs). Huaier is a commonly used Chinese patent medicine with substantial antitumor effects. The combination of Huaier and ICIs may increase the efficacy of ICIs against hepatocellular carcinoma (HCC).

Methods: The major components of Huaier were detected by high-performance liquid chromatography-mass spectrometry. The optimal antitumor dose of Huaier was investigated in H22-bearing mice. Next, Huaier was combined with anti-CD8α antibody (Ab) or anti-PD-L1 Ab to observe the antitumor effect. The safety of these combination drugs was evaluated through blood biochemical tests and hematoxylin and eosin staining of histological sections. RT-qPCR, immunohistochemistry, flow cytometry, and transcriptome sequencing were performed to investigate the potential action mechanism of anti-PD-L1 Ab combined with Huaier against HCC.

Results: HPLC-MS/MS identified 333 components of Huaier, including carboxylic acids and derivatives, thienothiophenes, phenols, flavonoids and so on. Huaier exhibited significant antitumor effects, with the strongest effect noted at a dose of 4 g/kg. Huaier boosted $CD8^+$ T cells infiltration into the tumor. Next, $CD8^+$ T cells were depleted by with anti-CD8α Ab, and the antitumor effect of Huaier was suppressed. Flow cytometry results revealed that $CD8^+$ T cells were reduced in the Huaier+anti-CD8α Ab group, with the antitumor effect of this group being inhibited. This indicated that $CD8^+$ T cells were key players in the antitumor activity of Huaier. Meanwhile, Huaier inhibited microvessel density (MVD), downregulated vascular endothelial growth factor A (VEGFA), and upregulated PD-L1 in tumor tissues. Finally, Huaier combined with anti-PD-L1 Ab exhibited a greater antitumor effect in the H22-bearing mice. And the results of liver and kidney function tests and histological section analysis unveiled that the safety of these drugs was excellent. According to the transcriptome sequencing results, Huaier combined with anti-PD-L1 Ab possibly exerted anti-HCC effects through immunomodulation, immune response, and so on.

Conclusions: Huaier exhibited a significant antitumor effect. It promoted $CD8^+$ T cells infiltration, upregulated PD-L1 expression, downregulated VEGFA expression, and inhibited MVD, thereby playing a significant antitumor immunoregulatory effect. The combination of Huaier and anti-PD-L1 Ab has significant antitumor effects, and this regimen has good safety. Therefore, Huaier combined with anti-PD-L1 Ab is a promising therapeutic approach against HCC.

Abbreviations: Ab, antibody; AOD, average optical density; ALT, alanine aminotransferase; AST, aspartate aminotransferase; BP, biological process; BUN, blood urea nitrogen; CC, cellular components; DCR, disease control rates; DEGs, differentially expressed genes; GO, Gene Ontology; HCC, hepatocellular carcinoma; HPLC-MS/MS, high-performance liquid chromatography-mass spectrometry; ICC, intrahepatic cholangiocarcinoma; ICIs, immune checkpoint inhibitors; IHC, immunochemistry; KEGG, Kyoto Encyclopedia of Genes and Genomes; MF, molecular function; MVD, microvessel density; ORR, objective response rates; OS, overall survival; PLC, primary liver cancer; Scr, serum creatinine; TIC, total ion chromatography; TME, tumor microenvironment; VEGFA, vascular endothelial growth factor A; TME, tumour microenvironment; TRAEs, treatment-related adverse events.

* Corresponding authors.
E-mail addresses: yangxi0073@163.com (X. Yang), yicheng6834@126.com (C. Yi).

[1] Equally contributed.

https://doi.org/10.1016/j.phymed.2023.155189
Received 21 August 2023; Received in revised form 31 October 2023; Accepted 3 November 2023
Available online 4 November 2023

Introduction

Primary liver cancer (PLC) is one of the most common malignant tumors worldwide. The pathologic types of PLC are intrahepatic cholangiocarcinoma (ICC), hepatocellular carcinoma (HCC), and other rare forms. Being the most common type, HCC accounts for 75%–85% of PLC (Sung et al., 2021). HCC is poorly prognostic and has a 5-year survival rate as low as 18% (Villanueva, 2019). The therapeutic effect of drugs against HCC must be urgently improved. Numerous studies have recently shown that immune checkpoint inhibitors (ICIs) possess significantly improved efficacy against HCC.

In the CheckMate-040 study, nivolumab achieved disease control rates (DCRs) and objective response rates (ORRs) of 58%–64% and 15%–20%, respectively (El-Khoueiry et al., 2017). In the KEYNOTE-224 study, the ORR of pembrolizumab as a second-line therapy was 18.3% (95% CI: 11.4–27.1) and the median overall survival (OS) was 13.2 months (95% CI: 9.7–15.3) (Zhu et al., 2018). As a second-line therapy, camrelizumab achieved an ORR and a median OS of 14.7% and 13.8 months, respectively (Qin et al., 2020). Furthermore, several ICIs monotherapies for HCC, such as durvalumab, tislelizumab, etc., have exhibited good clinical efficacy (Abou-Alfa et al., 2022; S. Qin et al., 2022). Compared with conventional chemotherapy or targeted therapy, ICIs monotherapy achieves a higher ORR, but it is still not ideal, with an ORR of $< 20\%$ (Ott et al., 2017).

In the IMbrave 150 study, the median OS of bevacizumab combined with atezolizumab and sorafenib was 19.2 months (95% CI: 17.0–23.7) and 13.4 months (95% CI: 11.4–16.9), respectively ($p < 0.001$). The combination therapy group had an ORR of 30%, which was significantly higher than that of single-agent immunotherapy (Cheng et al., 2022). In the CheckMate-040 study, nivolumab plus ipilimumab achieved an ORR of 32% (Yau et al., 2020). In a phase III study, camrelizumab combined with apatinib could prolonged median OS (22.1 months vs. 15.2 months, $p < 0.0001$) and improved ORR (25.4% vs. 5.9%, $p < 0.0001$) (S. Qin et al., 2022). Although the combination therapy improved ORR, it also increased adverse events. In the IMbrave 150 study, 43% of patients treated with the combination of atezolizumab and bevacizumab experienced grade 3–4 treatment-related adverse events (TRAEs), and 22% of patients were withdrawn from the study due to serious adverse events (Cheng et al., 2022). In a phase III clinical trial, camrelizumab plus apatinib resulted in grade 3 TRAEs in 80.9% of patients, of which 24.3% of patients discontinued treatment because of the TRAEs (S. Qin et al., 2022). In cohort 6 of the CheckMate-040 trial, the incidence of grade 3–4 TRAE was higher in patients treated with nivolumab plus cabozantinib and ipilimumab than in those treated with the two-drug regimen of nivolumab plus cabozantinib (74% vs. 50%) (Yau et al., 2022). Toxicity limits the use of the combination strategy. Therefore, finding a new combination therapy for augmenting ICIs efficacy with manageable toxicity is a crucial research component.

Huaier (*Trametes robiniophila* Murr) is a medicinal mushroom that has been documented to be used clinically for more than 1000 years in China. And Huaier is an extract separated and purified from *T. robiniophila Murr* that contains effective medicinal ingredients (Long and Wu, 2023; Jianwu et al., 2015). Huaier has various antitumor effects. For example, it promotes apoptosis of Hep-G2 cells (Ren et al., 2009), inhibits the proliferation of HUVEC cells, downgrades microvessel density (MVD) (Wang et al., 2012; Zou et al., 2015), reverses the resistance of drug-resistant cells to sorafenib and oxaliplatin (Tao et al., 2018; Zheng-guang et al., 2020), downregulates P53 (Xu et al., 2011), and regulates the NF-κB/IκBα signaling pathway and Yes-associated protein 1 to exert antitumor effects (Shan et al., 2017; Yang et al., 2017). Additionally, Huaier can activate the mTOR signaling pathway, increase tumor cell sensitivity to rapamycin and cisplatin (Hu et al., 2016), and regulate the AUF-1 signaling pathway to reduce SMMC-7721 cell metastasis (C. Li et al., 2015). At that same time, Huaier can also regulate immune functions. It can increase the thymus and spleen index of H22-bearing mice as well as the $CD3^+$T cell count and $CD4^+$ T/$CD8^+$ T cell ratio in HCC patients (C. Li et al., 2015; Xue-zheng et al., 2013). Sun Yi et al. found that a polysaccharide extracted from Huaier promoted the proliferation of mouse spleen cells and activated macrophages to produce nitric oxide, thereby playing an antitumor immunomodulatory role (Sun et al., 2013). In a phase III clinical trial of adjuvant therapy with Huaier following the radical resection of HCC, the Huaier group exhibited an improved recurrence-free survival rate compared with the control group (62.39% vs. 49.05%, $p = 0.0001$) (Chen et al., 2018). In a study combining Huaier with thermal ablation, the extrahepatic metastasis rate was significantly lower in the combined group than in the ablation alone group (HR = 0.49, 95% CI: 0.27–0.89, $p = 0.018$) (Wang et al., 2021). These studies have suggest that Huaier can exert an antitumor effect and can regulate immune organs and cells. Moreover, Huaier does not significantly increase side effects and has a good safety profile (Chen et al., 2018; Wang et al., 2021).

In the study, we first observed the antitumor effect of Huaier on H22-bearing mice, followed by the determination of the efficacy of Huaier against $CD8^+$ T cells. Then, $CD8^+$ T cells were eliminated with anti-CD8α Ab to explore the role of these cells in the antitumor effect of Huaier. Moreover, the effect of Huaier on VEGFA and PD-L1 expression and MVD was investigated. Finally, the combination of Huaier and ICIs was used in H22-bearing mice to observe the antitumor effect and explore the underlying action mechanism of this combination. The study's objective was to observe the therapeutic efficacy and safety of Huaier plus ICIs against HCC through animal studies and to investigate the potential action mechanism of this combination, which is of great clinical value.

Materials and methods

Identification of major chemical components

High-performance liquid chromatography-tandem mass spectrometry (HPLC-MS/MS) was performed to identify the chemical components of Huaier. HPLC-MS/MS was carried out by instrument analysis platform: LC-MS (Thermo, Ultimate 3000LC, Q Exactive HF), chromatographic column: C18 column (Zorbax Eclipse C18(1.8 μm × 2.1 mm × 100 mm)). The mass spectrometry ion source was electrospray ionization, and the scanning mode was a positive-negative ion switch scan.

Mice and cell lines

The H22 cell line was provided by Procell Life Science & Technology Co, LTD. Six-week-old male BALB/c mice (weight: 16 ± 2 g) were purchased from Beijing Huafukang Biotechnology Co., LTD and housed in cages under optimal conditions of light, temperature, and humidity. Five mice were housed in each cage, and adequate water and food were provided to the mice. This study received ethical approval from the Experimental Animal Ethics Committee of the West China Hospital of Sichuan University on March 17, 2021 (registration number: 20211128A).

Establishment of the H22-bearing mouse model

H22 cells were collected and prepared into a single cell suspension containing 2×10^7 cells/ml. Then, 1×10^7 cells were inoculated on the right back of the mice. The tumor volume was measured each 3 days. About 1 week later, the mice were randomly grouped based on their tumor volumes and subjected to pharmacological intervention.

The experiment of different doses of Huaier (Qidong Gai Tianli Pharmaceutical Co., LTD., BC17, China) to intervene in H22-bearing mice was divided into model group, Huaier 1 g/kg group, Huaier 2 g/kg group and Huaier 4 g/kg group, with 5 mice included in each group. The model group was given 0.2 ml saline through gavage once every 2 days. The different doses of the Huaier solution (0.2 ml) were administered to the Huaier groups through gavage once every 2 days. These

treatments lasted for 21 days.

The experiment of Huaier and anti-CD8α antibody (Ab) (Univ, BE0004–1, USA) in the treatment of H22-bearing mice was divided into model group, Huaier group, anti-CD8α Ab group, and Huaier+anti-CD8α Ab group, with 5 mice included in each group. The model group was given 0.2 ml saline through gavage once every 2 days. The Huaier group received 0.2 ml of 4 g/kg Huaier solution through gavage once every 2 days. In the anti-CD8α Ab group, 50 μg anti-CD8α Ab was intraperitoneally injected into the mice twice a week. The Huaier+anti-CD8α Ab group received the same dose of Huaier and anti-CD8α Ab. These treatments lasted for 21 days.

The experiment of Huaier combined with anti-PD-L1 Ab (Univ, BE0101, USA) in the treatment of H22-bearing mice was divided into model group, Huaier group, anti-PD-L1 Ab group and Huaier+anti-PD-L1 Ab group, with 5 mice included in each group. The model group was given 0.2 ml saline through gavage once every 2 days. The Huaier group received 0.2 ml of 4 g/kg Huaier solution through gavage once every 2 days. The anti-PD-L1 Ab group was injected intraperitoneally with 100 μg anti-PD-L1 Ab once every 3 days. The Huaier+anti-PD-L1 Ab group received the same dose of Huaier and anti-PD-L1 Ab. These treatments lasted for 21 days.

Liver and kidney function tests

Blood from the mice was withdrawn and collected. Using test kits provided by Radu Life Sciences, some tests were conducted to examine for indicators, including aspartate aminotransferase (AST), alanine aminotransferase (ALT), serum creatinine (Scr), and blood urea nitrogen (BUN). Accordingly, the sample collected was subjected to the aforementioned tests on a fully automated biochemistry instrument after setting the appropriate parameters.

Hematoxylin and eosin staining of histological sections

Mouse heart, lung, liver, spleen, and kidney tissues were fixed, embedded, and sectioned, and hematoxylin and eosin (HE) staining was performed using the HE stain kit (Solarbio, G1120, China). Finally, the stained tissues were observed under a microscope (Olympus Corporation, Japan), and appropriate photographs were taken.

Flow cytometry assays

Mouse spleen was prepared as single cell suspension. The suspension was then processed with red blood cell lysis buffer (Beijing Coolaber Technology Co., SL1070, China). Next, FITC antimouse CD3 Ab (Elabscience, E-AB-F1013C, China), APC antimouse CD4 Ab (Elabscience, E-AB-F1097E, China), and PE antimouse CD8a Ab (Elabscience, E-AB-F1104D, China) were added to the lysed suspension for staining. Finally, all samples were run on a NovoCyte Advanteon flow cytometer (Agilent Technologies, Inc., USA).

Quantitative real-time PCR analysis

Tumour tissues were used as the test sample. An animal total RNA isolation kit (Foregene, RE-03,011, China) was used to extract RNA and cDNAs were synthesized by using the RT easy TM II kit (Foregene, RT-01,031, China). PD-L1 and VEGFA mRNA was detected using a real-time PCR easy TM-SYBR green I kit (Foregene, QP-01,012, China). The primers used for qPCR in this study are listed Table 1.

Immunohistochemistry

To analyze CD8, CD31, VEGFA, and PD-L1 expression in tumor tissues, immunochemistry (IHC) was performed using the standard method. The primary antibodies used were as follows: anti-CD8 alpha Ab (Abcam, ab217344, USA), anti-VEGFA Ab (ABclonal, A12303, China), anti-CD31 Ab (Abcam, ab182981, USA), and anti-PD-L1 Ab (Bioss, bs-1103R, China). Finally, the positively stained area was photographed under a microscope.

To analyze $CD8^+$ T cells, positive cells were counted by selecting five high-magnification (×400) fields for each section. Cells stained brownish yellow were considered positive.

Average optical density (AOD) was used to analyze VEGFA and PD-L1 expression (Yang et al., 2007). Five high-magnification (× 400) fields were selected for each section. The image was processed using ImageJ software to obtain the area and IntDen information of the image. Area is the number of positive pixels in the image, and IntDen is the total optical density value. The IntDen to area ratio is AOD.

MVD was evaluated through anti-CD31 Ab staining, and IHC staining was considered positive when it was brownish. The highest vascular density area within the tumor was first searched at low magnification (×40), and then, five high-magnification (× 400) fields were selected. The mean of microvessel counts within the field of view was considered as MVD (Weidner et al., 1992).

Reference transcriptome sequencing of tumor tissue

The samples for sequencing were tumor tissues from the model and Huaier+anti-PD-L1 Ab groups. Tissue RNA was extracted using TRIzol (Thermo Fisher, 15,596,018, USA). After two rounds of purification with oligo(dT) magnetic beads (Thermo Fisher, 25–61,005, USA), mRNA with a poly-A tail was obtained and then fragmented using the Magnesium RNA Fragmentation Module kit (NEBNext, E6150S, USA). The fragmented RNA was synthesized into cDNA by using reverse transcriptase (Invitrogen, 1,896,649, USA). Next, two-strand synthesis is performed to convert these complex double strands of DNA and RNA into DNA double-strands. A dUTP solution (Thermo Fisher, R0133, USA) was then applied to the double-stranded DNA duplexes to align their ends. After an A base was attached to each end to allow ligation to a connector with a T base, magnetic beads were used to check and purify the fragment size. Consequently, the second strand was digested with UDGase (NEB, m0280, USA), and PCR was performed to generate a library. Finally, the library was sequenced using LC Bio-Technology NovaseqTM 6000 (LC Bio-Technology CO., Ltd., China).

Once the downstream sequencing data were obtained, they were screened to obtain high-quality sequencing data. These data were then compared to the reference genome of the species in this project and analyzed for gene expression. Then, differentially expressed genes (DEGs) were screened considering $|\log_2 FC| \geq 1$ and $q < 0.05$. Histograms and volcano plots of the DEGs were plotted. Gene Ontology (GO) and Kyoto Encyclopedia of Genes and Genomes (KEGG) enrichment analyses were performed.

Data statistics and analysis

The measured data were expressed as the mean ± SD. A *t*-test or ANOVA was performed for statistical analysis, with $p < 0.05$ considered statistically significant. GraphPad Prism 8.0, ImageJ, and Adobe Photoshop 2019 software were used for data and image processing.

Table 1
The primers used for qPCR in this study.

Gene	Forward primer(5′→3′)	Reverse primer(5′→3′)
GAPDH	AGGTCGGTGTGAACGGATTTG	GGGGTCGTTGATGGCAACA
VEGFA	CTGCTCTCTTGGGTGCACTG	GCAGCCTGGGACCACTTG
PD-L1	GCTCCAAAGGACTTGTACGTG	TGATCTGAAGGGCAGCATTTC

Results

Identification of compounds in Huaier

The total ion chromatography (TIC) of Huaier is shown in Fig. 1. And a total of 333 compounds were obtained by compositional resolution of positive and negative ion patterns, including carboxylic acids and derivatives (A), thienothiophenes (B), organooxygen compounds (C), carboxylic acids and derivatives (D), organonitrogen compounds (E), flavonoids and so on. All the compounds were showed in supplementary Table 1.

Huaier inhibits the growth of H22-bearing mice

The antitumor effect of Huaier was investigated using H22-bearing mice. Depending on the group assigned to, saline or 1, 2, or 4 g/kg body weight dose of Huaier was administered to the mice from day 1 to day 21 (Fig. 2A). Huaier inhibited the growth of H22 mice. Tumor growth curves and relative tumor volume curves were presented in Fig. 2B and C. Supplementary Fig. 1 presents tumor images after treatment and tumor weights. The results revealed that Huaier had a remarkable antitumor effect, with the tumor volume in the Huaier 4 g/kg group being the smallest. The mean tumor volume on day 21 was 1033.91 ± 490.50 mm^3 in the model group, 1024.59 ± 244.36 mm^3 in the Huaier 1 g/kg group, 714.62 ± 134.65 mm^3 in the Huaier 2 g/kg group, and 417.81 ± 112.14 mm^3 in the Huaier 4 g/kg group. The mean tumor volume in the Huaier 4 g/kg group was 59.60% lower than that in the model group. Next, the safety of the combination therapy was evaluated. The evaluated test indicators (AST, Scr, ALT, and BUN) of the mice in each group fluctuated within the normal range (supplementary Fig. 2A). Histological sections exhibited no significant pathological changes in each group (supplementary Fig. 2B).

Huaier promotes $CD8^+$ T cells infiltration

$CD8^+$ T cells are critical cells in the antitumor immune response. To observe the regulatory effect of Huaier on $CD8^+$ T cells, the number of $CD8^+$ T cells was examined. Fig. 3A and B present the flow cytometry

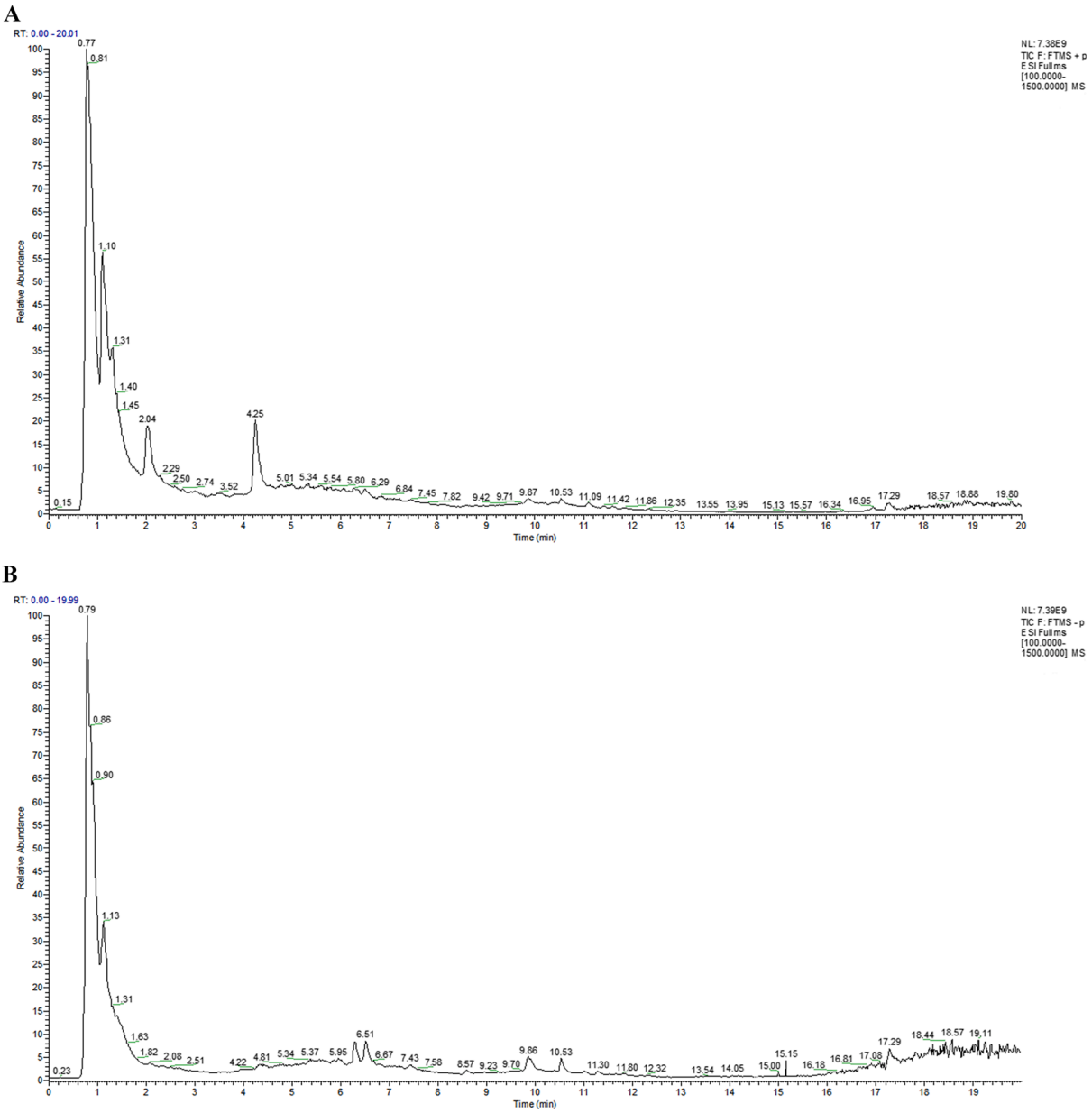

Fig. 1. The TIC of Huaier. (A) Positive mode. (B) Negative mode.

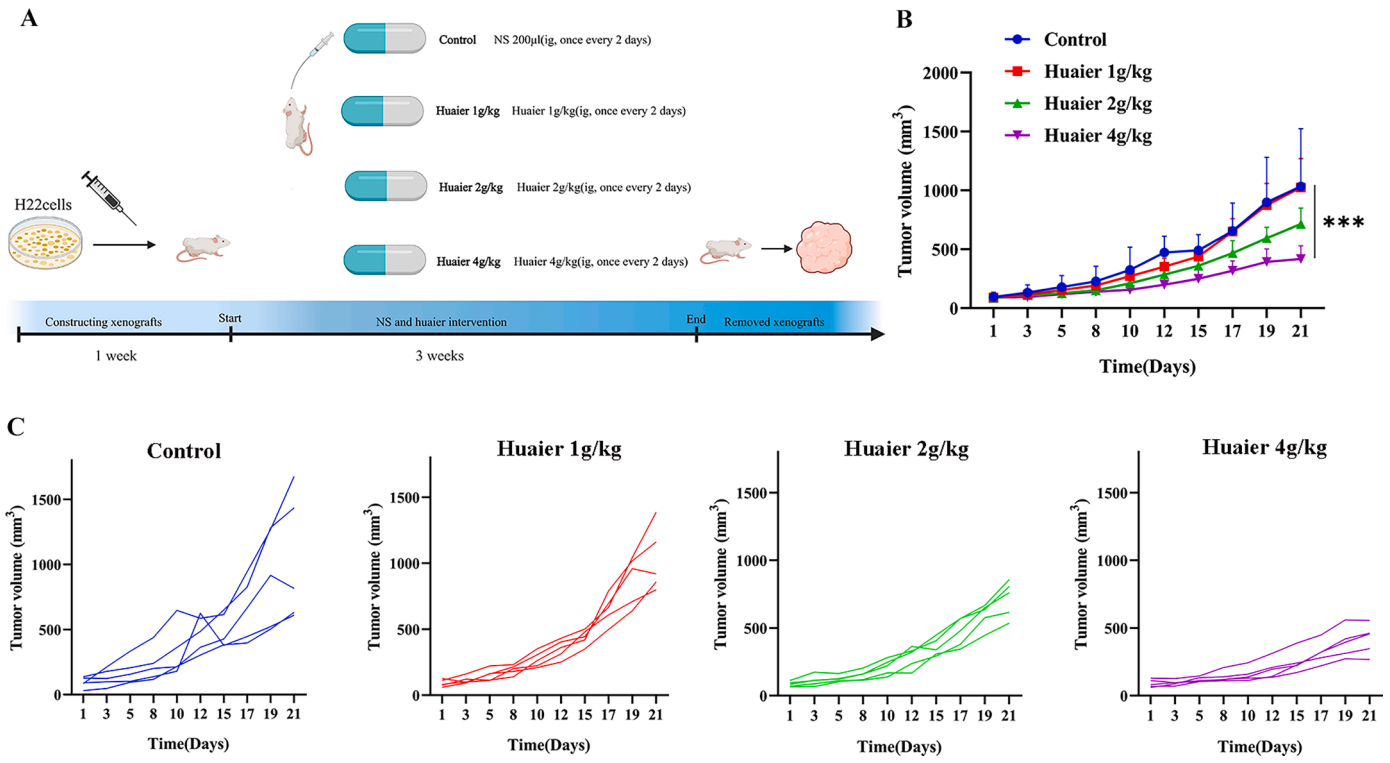

Fig. 2. The efficacy of Huaier on H22-bearing mice. (A) The scheme of tumor inoculation and treatment. H22 tumor cells were injected into male BALB/c mice subcutaneously. After 1 week, 4 groups of H22-bearing mice were administered saline, Huaier via gavage. (B) The tumor volume in different groups ($n = 5$). (C) Relative tumor volume curves in different groups ($n = 5$). ***$p < 0.001$ was considered to indicate statistical significance.

results, the number of $CD8^+$ T cells in the Huaier group was higher than that in the model group ($p < 0.05$). Fig. 3C and D present the IHC results, the number of $CD8^+$ T cells was also higher in the Huaier group than in the model group ($p < 0.0001$). These results indicated that Huaier promoted the infiltration of $CD8^+$ T cells.

$CD8^+$ T cells are crucial immune cells for Huaier to exert the antitumor effect

$CD8^+$ T cells play a crucial antitumor immunomodulatory role. Meanwhile, Huaier can promote $CD8^+$ T cells infiltration. Therefore, we hypothesized that $CD8^+$ T cells are key cells involved in the antitumor

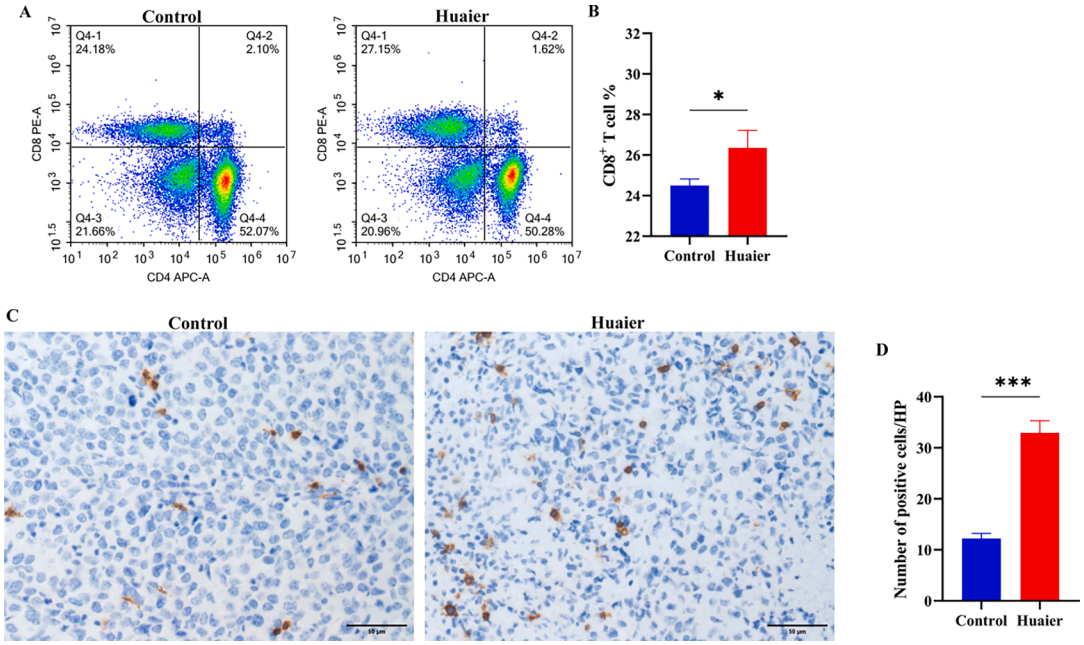

Fig. 3. Huaier promoted the infiltration of $CD8^+$ T cells in H22-bearing mice. (A–B) Flow cytometry was used to detect $CD8^+$ T cells in the mice spleen. The bar graph depicts the percentage of $CD8^+$ T cells. (C–D) IHC was performed to detect the staining outcomes of $CD8^+$ T cells in the tumor tissues of the experimental mice. The bar graph depicts the amount of $CD8^+$ T cells. *$p < 0.05$ and ***$p < 0.001$ were considered to indicate statistical significance.

effect of Huaier. In this experiment, $CD8^+$ T cells were depleted using anti-CD8α Ab, and changes in the antitumor effect of Huaier were observed. Fig. 4A presents the schematic diagram of tumor inoculation and treatment. Following 21 days of Huaier and anti-CD8α Ab intervention, tumor growth curves and relative tumor volume curves are presented in Fig. 4B and C. Supplementary Fig. 3 presents tumor images after treatment and tumor weights. Although there was no statistical difference in tumor volume among the four groups, the tumor volume was lowest in the Huaier group. The tumor volumes increased in the anti-CD8α Ab groups and Huaier+anti-CD8α Ab groups compared with the Huaier group and were close to that in the model group. On combining the tumor weight and tumor volume of each group, we noted that the antitumor effect of Huaier reduced after the anti-CD8α Ab intervention. The flow cytometry result revealed that the number of $CD8^+$ T cells in the Huaier group was the highest. After intervention with anti-CD8α Ab, the number of $CD8^+$ T cells in the anti-CD8α Ab group and Huaier+anti-CD8α Ab groups decreased significantly (Fig. 4D and E), with the disappearance of the antitumor effect in these two groups. Thus, the results confirmed that $CD8^+$ T cells are crucial immune cells for the antitumor effect of Huaier.

Huaier regulates MVD, VEGFA, and PD-L1 expression in tumor tissues

VEGFA, an essential angiogenic factor, is highly correlated with tumor angiogenesis. In this study, VEGFA mRNA (Fig. 5A) and VEGF AOD (Fig. 5C and D) decreased in the Huaier group ($p < 0.01$ and $p < 0.05$, respectively). The CD31 staining result is presented in Fig. 5E and F. MVD significantly decreased in the Huaier group ($p < 0.0001$). According to these results, Huaier can downregulate VEGFA expression and inhibit MVD.

PD-L1, a key immunosuppressive molecule, is a crucial prognostic indicator of immunotherapy efficacy. In this study, PD-L1 mRNA in tumor tissues was upregulated in the Huaier group ($p < 0.05$) (Fig. 5B). PD-L1 AOD was also higher in the Huaier group ($p < 0.0001$) (Fig. 5G and H). These results suggestedthat Huaier can upregulate PD-L1 expression in the tumor tissue.

Huaier combined with anti-PD-L1 Ab enhances the antitumor effect

Combining drugs with ICIs has become an effective method of improving efficacy. Because Huaier can upregulate PD-L1 expression, it may improve the sensitivity of malignant tumors to anti-PD-L1 Ab. Therefore, we investigated whether Huaier could improve the efficacy of anti-PD-L1 Ab in the treatment of HCC. The scheme of tumor inoculation and treatment is presented in Fig. 6A. Fig. 6B and C present tumor volume curves and relative tumor volume curves. Tumor images after treatment and tumor weights were shown in supplementary Fig. 4. The tumor growth rate was the fastest in the model group, with the tumor volume and weight being the largest. Compared with the model group, tumor volume was reduced in the Huaier and anti-PD-L1 Ab groups ($p < 0.05$ and $p < 0.001$, respectively) (Fig. 6). The antitumor effect was further increased and the tumor volume was the lowest in the Huaier+anti-PD-L1 Ab group, and the difference was significant compared with the model group ($p < 0.0001$). On comparing the mean tumor volume on day 21, we noted that the mean tumor volume was 1008 ± 322.82 mm^3 in the model group, 656.34 ± 120.56 mm^3 in the Huaier group, 488.07 ± 209.94 mm^3 in the anti-PD-L1 Ab group, and 198.33 ± 110.68 mm^3 in the Huaier+anti-PD-L1 Ab group. The mean tumor volume was reduced by 80.32% in the Huaier+anti-PD-L1 Ab group compared with the model group. These results revealed that the Huaier+anti-PD-L1 group had the best antitumor effect. Next, the safety of the combination therapy was evaluated. The evaluated test indicators (AST, ALT, Scr, and BUN) of mice in each group fluctuated within the normal range (supplementary Fig. 5A). Histological sections revealed no significant pathological changes in each group (supplementary Fig. 5B).

Potential action mechanism of Huaier combined with anti-PD-L1 Ab for HCC treatment

To reveal the possible action mechanism of the Huaier combined with anti-PD-L1 Ab in the treatment of HCC, transcriptome sequencing of tumor tissue was performed. DEGs were first screened considering $|\log2FC| \geq 1$ and $q < 0.05$, and the histogram and volcano plot of DEGs were plotted (Fig. 7). The DEGs were genes that met the differential multiplicity and significant level among genes obtained from different treatment samples, including upregulated and downregulated genes. Differential gene analysis can help determine the expression of genes between different groups, which is of great significance in revealing the action mechanism of a drug.

Next, these DEGs were used for GO and KEGG analyses. The GO enrichment analysis includes: biological processes (BP), cellular components (CC), and molecular function (MF). These categories are used to functionally annotate genes in terms of their function, biological pathway, and localization in cells, respectively (Consortium, 2017). Of the categories, BP included the immune system process, inflammatory response, immune response, apoptotic process, etc. CC included the membrane, plasma membrane, cytoplasm, extracellular region, etc. MF included protein binding, hydrolase activity, G protein-coupled receptor activity, ATP binding, etc. These results are presented in Fig. 8A.

The action mechanism in organisms is complex, and numerous genes interact with each other to perform their biological functions. The KEGG analysis helps in understanding the biological functions of genes. The KEGG database is a comprehensive database of large-scale molecular data sets providing molecular-level information, especially those related to genome sequencing and other high-throughput generation. These data can be used to determine the advanced functions and benefits of cells, organisms, and ecosystems. Through this database, the pathways of target genes can be explored, and richer and more detailed bioinformatics content can be provided. Fig. 8B showed that the KEGG results included six levels. Among them, cellular processes included necroptosis, apoptosis, and ferroptosis. Environmental information processing included the MAPK signaling pathway, cytokine-cytokine receptor interaction, etc. Genetic information processing included ubiquitin-mediated proteolysis and protein processing in the endoplasmic reticulum. Metabolism included metabolic pathways, purine metabolism, and arginine and proline metabolism. Human diseases include pathways in cancer and rheumatoid arthritis. Organismal systems included the NOD-like receptor signaling pathway, chemokine signaling pathway, and IL-17 signaling pathway.

Discussion

ICIs are a great advancement in the history of tumor therapy. They have significantly improved antitumor efficacy, but their effectiveness when administered alone to treat HCC is < 20% (Ott et al., 2017). Combination therapy has become an indispensable method for improving the efficacy of drugs, including ICIs. In China, combining ICIs with Chinese medicine is a common treatment strategy.

In this study, Huaier exhibited a remarkable antitumor efficacy in H22-bearing mice. The inhibitory effect increased with an increase in the Huaier dose, with Huaier 4 g/kg exhibiting the strongest antitumor effect. Meanwhile, some test indicators (AST, ALT, Scr, and BUN) and histological sections of major organs exhibited no significant toxicity of Hauier in H22-bearing mice. Therefore, this study demonstrated that Huaier would be a promising and good safety drug for HCC treatment in H22-bearing mice.

According to the current study, Huaier can exert significant regulatory effects on immune organs, immune cells, and cytokines. Therefore, we speculated that Huaier may exert antitumor effects through immune regulation. $CD8^+$ T cells are crucial immune cell, the number of infiltrating $CD8^+$ T cells in the tumor is associated with tumor prognosis (Fridman et al., 2012). In this study, the results unveiled that Huaier

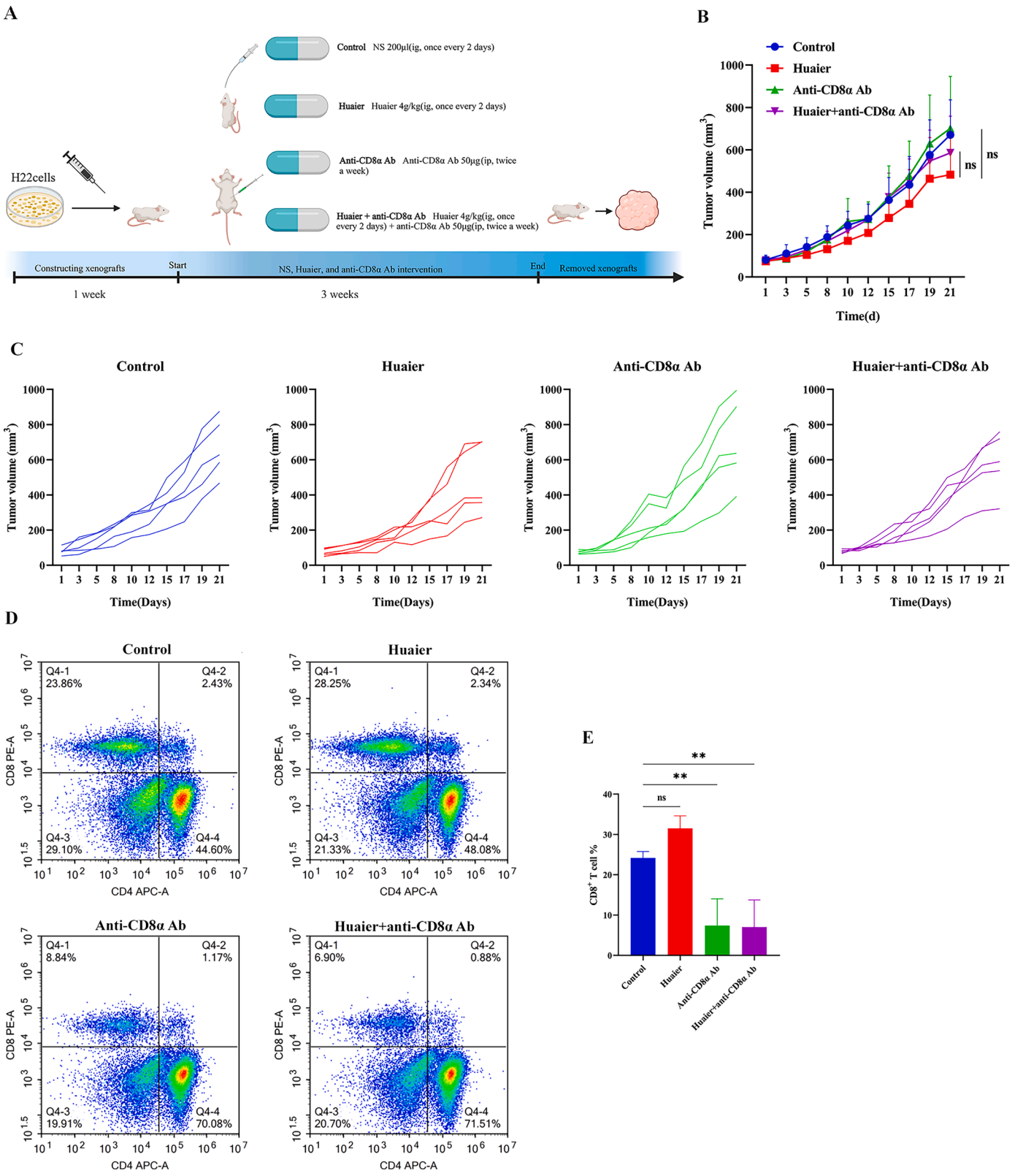

Fig. 4. The efficacy of Huaier in combination with anti-CD8α Ab on H22-bearing mice. (A) The scheme of tumor inoculation and treatment. H22 tumor cells were injected into male BALB/c mice subcutaneously. After 1 week, four groups of H22-bearing mice were administered saline, Huaier, and anti-CD8α Ab. (B) Tumor volume in different groups ($n = 5$). (C) The relative tumor volume curves in different groups ($n = 5$). (D–E) Flow cytometry detection of splenic $CD8^+$ T cells (D), the bar graph displays the percentage of $CD8^+$ T cells (E). $^{**}p < 0.01$ was considered to indicate statistical significance; ns = no significant difference.

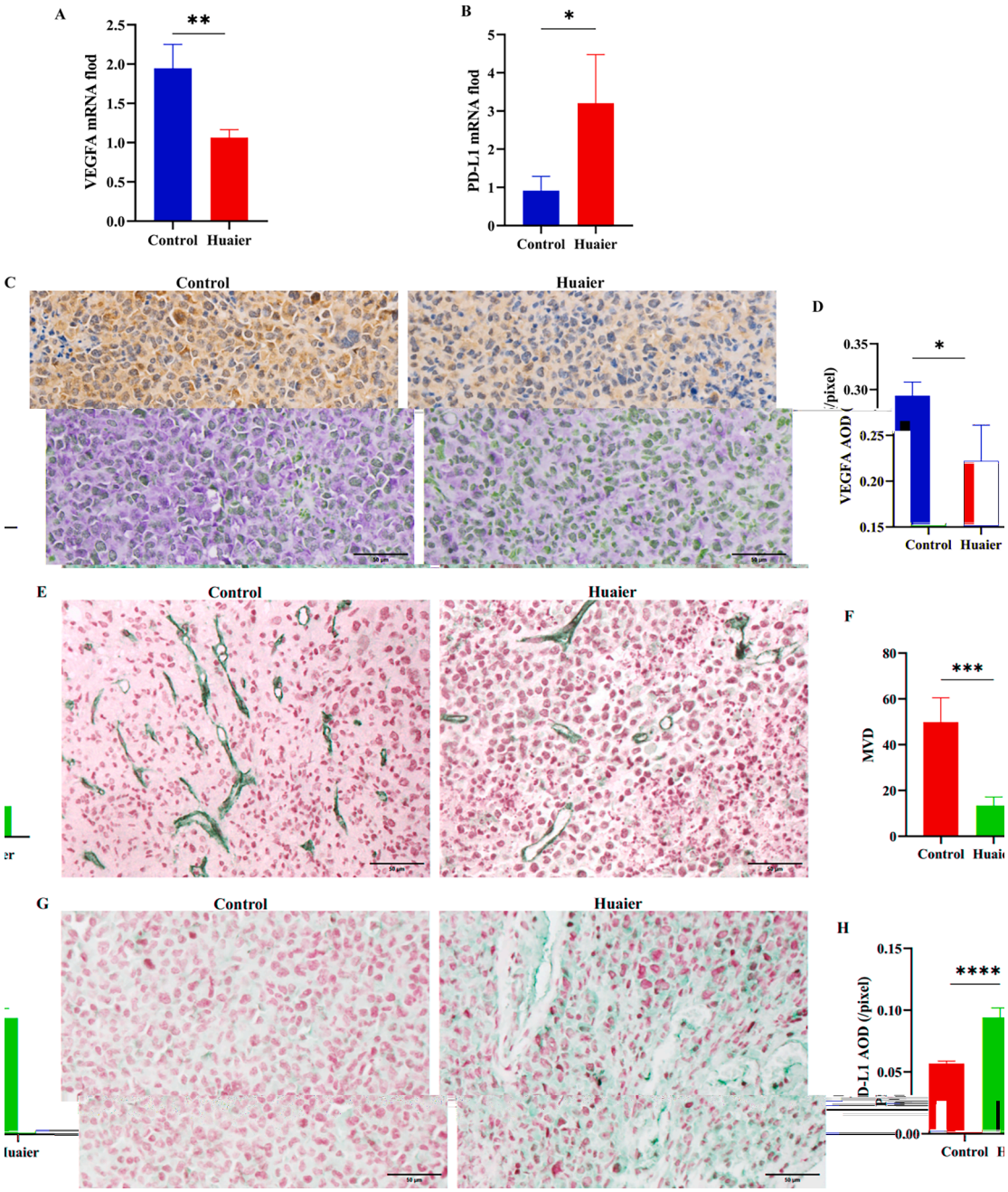

Fig. 5. Huaier regulated MVD and the expression of VEGFA and PD-L1. (A) Huaier downregulates the VEGFA expression in tumor tissues. (B) Huaier upregulates the PD-L1 expression in the tumor tissues. (C–D) IHC was applied to detect the staining result of VEGFA in the tumor tissues. The bar graph depicts the AOD values of the two groups. (E–F) IHC was used to detect the staining result of CD31 in the tumor tissues. The bar graph depicts the MVD of the two study groups. (G–H) IHC was applied to detect the staining results of PD-L1 in the tumor tissues. The bar graph displays the MVD of the two groups. *$p < 0.05$, **$p < 0.01$, and ***$p < 0.001$ were considered to indicate statistical significance.

could promote $CD8^+$ T cells infiltration into tumor. Given the importance of $CD8^+$ T cells in antitumor activity, this cell is hypothesized to be a key cell in the antitumor effect of Huaier. To verify this hypothesis, we used anti-CD8α Ab to antagonize $CD8^+$ T cells in mice. After 21 days of intervention with Huaier and anti-CD8α Ab, although no statistical differences in tumor volume were noted between the groups, the Huaier group exhibited the lowest tumor volume. Tumor volumes in the anti--CD8α Ab and Huaier+anti-CD8α Ab groups were close to that in the model group. According to the analysis of tumor volume and weight, the antitumor effect of Huaier significantly reduced after the anti-CD8α Ab intervention. The flow cytometry results revealed that the number of $CD8^+$ T cells was the highest in the Huaier group, whereas that in the anti-CD8α Ab and Huaier+anti-CD8α Ab groups significantly decreased after the anti-CD8α Ab intervention. Based on the tumor volume and flow cytometry results, we concluded that the decrease in the number of $CD8^+$ T cells was consistent with the reduced antitumor effect of Huaier. Moreover, we accordingly speculated that $CD8^+$ T cells are important cells for the antitumor effect of Huaier.

Tumor angiogenesis is among the characteristics of malignant tumors, and tumor vasculature promotes tumor growth and metastasis and inhibits the delivery of antitumor drugs, while also inhibiting the tumor microenvironment (TME). Antiangiogenic drugs can induce normalization of the tumor vasculature and convert the immunosuppressive-oriented TME into a TME with a predominantly antitumor effect

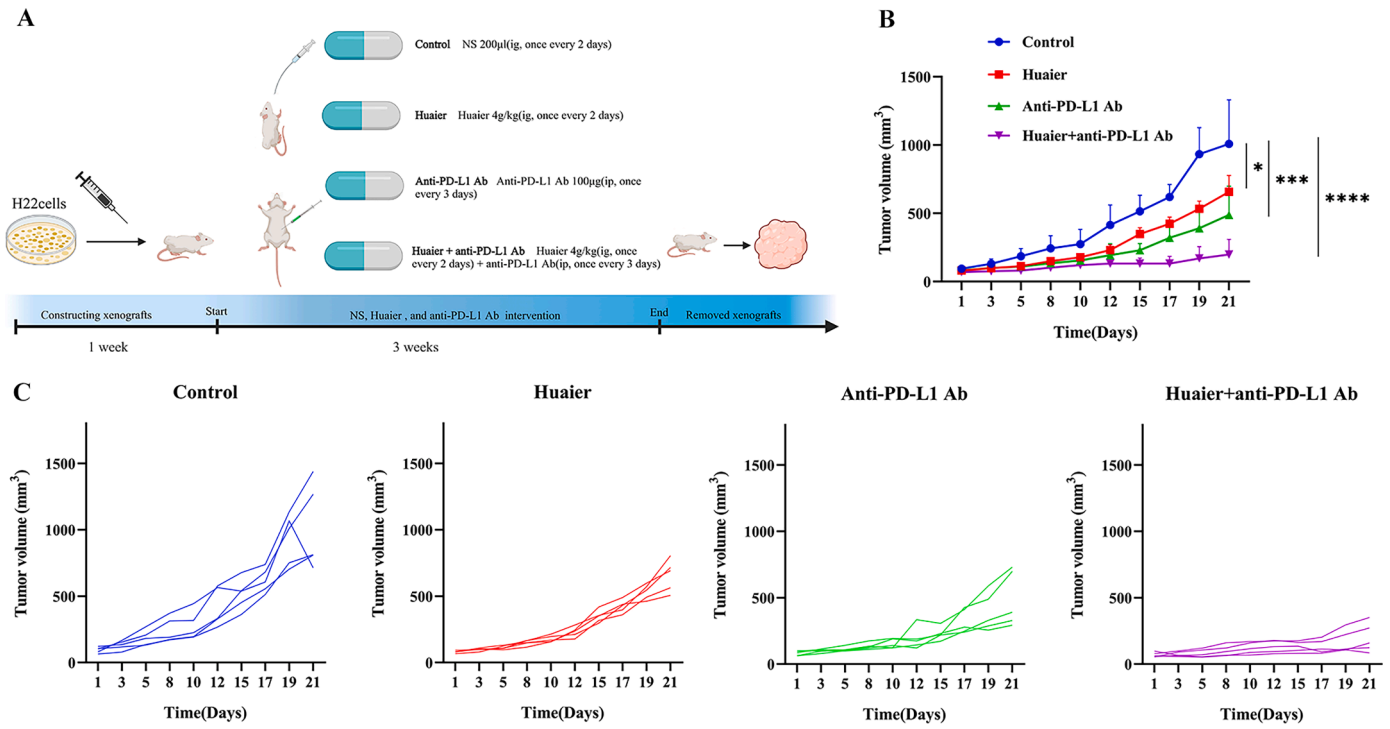

Fig. 6. The efficacy of Huaier in combination with anti-PD-L1 Ab on H22-bearing mice. (A) The scheme of tumor inoculation and treatment. H22 tumor cells were injected into male BALB/c mice subcutaneously. After 1 week, four groups of H22-bearing mice were administered saline, Huaier, and anti-PD-L1 Ab. (B) Tumor volume in different groups ($n = 5$). (C) The relative tumor volume curves in different groups ($n = 5$). $^{*}p < 0.05$, $^{***}p < 0.001$, and $^{****}p < 0.0001$ were considered to indicate statistical significance.

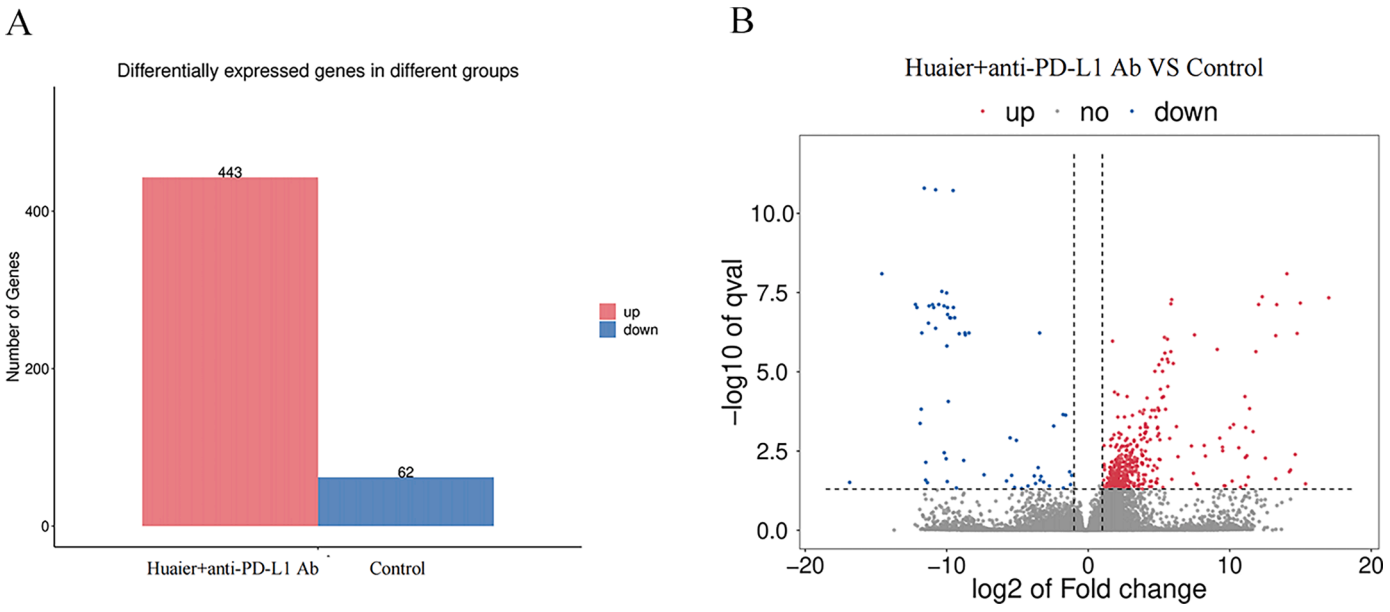

Fig. 7. DEGs in the Huaier and Huaier+anti-PD-L1 groups. A: Bar chart for DEGs; B: Volcano plot for DEGs.

(Deng-xuan et al., 2023). Therefore, antiangiogenic therapy is among the pivotal approaches for tumor treatment. In this study, Huaier downregulated VEGFA expression in tumor tissues. VEGF is a crucial pro-angiogenic factor that consists mainly of several members such as VEGFA, VEGFB, VEGFC, VEGFD, and VEGF-E. Among the members, VEGFA is a critical player in malignant tumor angiogenesis (Melincovici et al., 2018). Additionally, Huaier inhibited CD31 expression in tumor tissues. CD31 is commonly used to observe vascular endothelial cells and assess microangiogenesis in tissues. It is a common indicator used for studying tumor MVD (Franz et al., 2021). In this study, Huaier downregulated VEGFA expression and inhibited MVD, which suggested that Huaier exerts an antiangiogenic effect. Zhao Sha et al. exhibited that the combination of apatinib, a targeted antiangiogenic drug, and PD-L1 Ab enhances the antitumor effect, and its action mechanism is closely related to a reduction in the immunosuppressive microenvironment and an enhancement of the antitumor immune response (Zhao et al., 2017). These results suggested a potential synergistic effect of the antiangiogenic drug in combination with ICIs. Therefore, given the antitumor and antiangiogenic effects of Huaier, the Huaier and ICI combination has the potential benefit of increased efficacy.

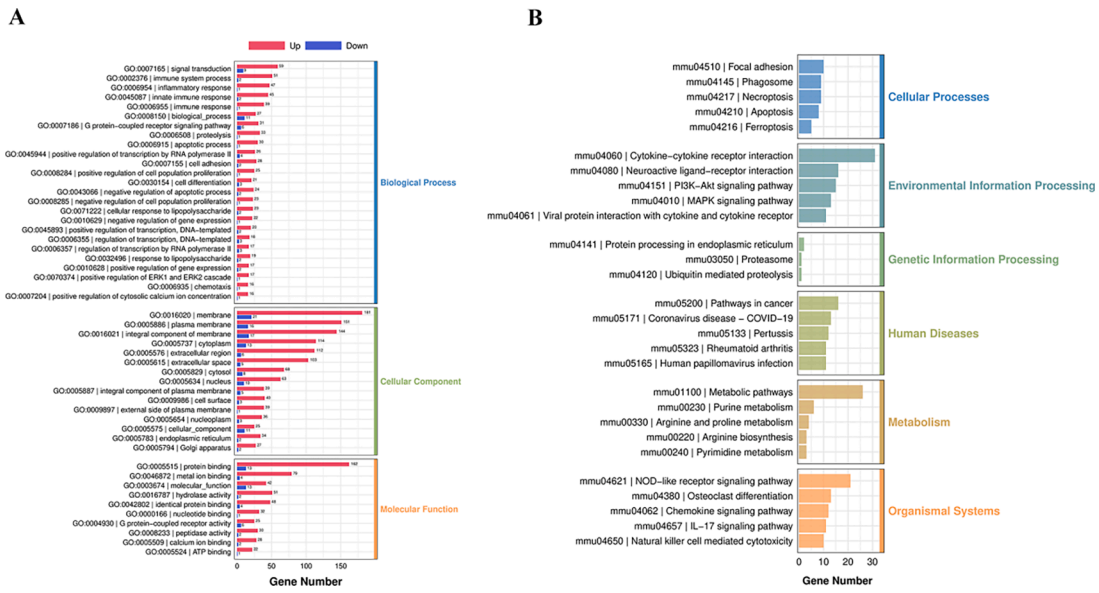

Fig. 8. GO enrichment barplot and KEGG enrichment barplot of DEGs.

PD-L1 is a critical immune checkpoint that significantly affects the efficacy of ICIs. This study found that Huaier promotes PD-L1 expression. This is because Huaier promoted the increase in the number of $CD8^{+}$T cells, and the increased $CD8^{+}$ T cells induced the increase in PD-L1 expression through the IFN-γ pathway (Ai et al., 2020; Alspach et al., 2019). At the same time, Huaier can induce the release of some inflammatory factors, such as IL-2 and TNF-α. These released inflammatory factors stimulated the increase in PD-L1 expression (Akhtar et al., 2021; Long and Wu, 2023; Narayanan et al., 2023).

As a vital immune checkpoint, PD-L1 exerts a negative regulatory effect on T cells. The downregulated PD-L1 expression releases the anticancer "brake" of the immune system, but the upregulated PD-L1 expression can turn cold tumors into hot tumors and boost the effect of ICIs (Wu et al., 2022). Su et al.'s study showed that the use of anlotinib could upregulate PD-L1 expression, and the combination of anlotinib with PD-1 checkpoint blockade could significantly enhance the antitumor effect against neuroblastoma. Thus, increasing PD-L1 may enhance the efficacy of ICIs. (Su et al., 2022). Morita Masahiro et al. analyzed the clinical information of 34 patients with advanced HCC who were treated with PD-1 Ab. The results showed that patients with increased $CD8^{+}$ T cells and high PD-L1 expression had better progression-free survival, OS, and DCR (Morita et al., 2021). Our results also exhibited that increased $CD8^{+}$ T cells and PD-L1 expression in the Huaier group were strongly associated with better antitumor efficacy.

Based on the aforementioned results, we concluded that Huaier promoted $CD8^{+}$ T cell infiltration and downregulated the expression of VEGFA and CD31, which played an antitumor angiogenesis role. Meanwhile, Huaier upregulated PD-L1 expression and changed the "cold tumor" into a "hot tumor". These effects are essential for improving the immune microenvironment and enhancing the efficacy of ICIs. Therefore, we hypothesized that Huaier combined with anti-PD-L1 Ab improves efficacy.

To confirm this hypothesis, we combined Huaier and anti-PD-L1 Ab and used it for HCC treatment. After 21 days of intervention, the model group exhibited the largest tumor volume, which was suppressed in both Huaier and anti-PD-L1 Ab groups. Among them, the Huaier+anti-PD-L1 Ab group exhibited the strongest antitumor effect. Meanwhile, some test indicators (AST, ALT, Scr, and BUN) and histological sections of major organs revealed no significant toxicity of Hauier in H22-bearing mice, thereby suggesting a good safety profile for this treatment. These results demonstrated that the increased infiltration of immune cells in tumors and the upregulated PD-L1 expression in the TME made the tumors more sensitive to ICIs and improved the antitumor efficacy of anti-PD-L1 Ab (Han et al., 2019; Wei et al., 2022). Meanwhile, Huaier also exhibited an antiangiogenic effect, which is valuable for increasing the efficacy of ICIs. Fig. 9 shows the immunomodulatory effect of Huaier and Huaier improves the efficacy of anti-PD-L1 Ab in treating HCC.

To further reveal the potential action mechanisms of the Huaier and anti-PD-L1 Ab combination in HCC treatment, reference transcriptome sequencing was performed. Transcriptome sequencing is used to determine the expression, structure, and interaction of genes at the whole level. This sequencing is valuable for clarifying the mechanism of interaction between organisms and is therefore widely used in various fields of life science. In this study, 443 and 62 upregulated and downregulated genes, respectively, were screened on the basis of the criteria of $|\log_2 FC| \geq 1$ and $q < 0.05$. These genes are considered crucial in HCC treatment with the Huaier and anti-PD-L1 Ab combination. These DEGs were then used for the GO and KEGG enrichment analyses. In GO enrichment, the DEGs were mainly enriched in immune regulation, inflammatory response, cell signaling, proliferation, and apoptosis, which was generally consistent with the present study results. This further confirmed that Huaier combined with anti-PD-L1 Ab exerts antitumor effects through immune regulation, inflammatory responses, and other processes. In the KEGG enrichment analysis, the pathways significantly enriched were the cytokine-cytokine receptor interaction, PI3K-Akt signaling pathway, etc.

The aforementioned studies have clarified that Huaier can exert anti-HCC effects by promoting $CD8^{+}$ T cell infiltration, downregulating VEGFA expression, inhibiting MVD, and upregulating PD-L1. Thus, Huaier possesses significant immunomodulatory effects and is promising in increasing the efficacy of anti-PD-L1 Ab. The results also confirmed that the Huaier and anti-PD-L1 Ab combination can enhance the antitumor effect.

Animal experiments conducted in this study revealed that Huaier has significant immunomodulatory effects. Huaier was then combined with anti-PD-L1 Ab for HCC treatment. The combination therapy increased the anti-HCC efficacy of anti-PD-L1 Ab. This study, for the first time, demonstrates that the Huaier and anti-PD-L1 Ab combination is a very valuable therapeutic option. Of course, the present study has some limitations. We here aimed to determine the therapeutic efficacy of the anti-PD-L1 Ab and Huaier combination against HCC. Tumors in the combined group exhibited a continuous shrinking trend during the observation period. However, the study currently lacks investigations on HCC recurrence and delayed adverse events, and these are among the

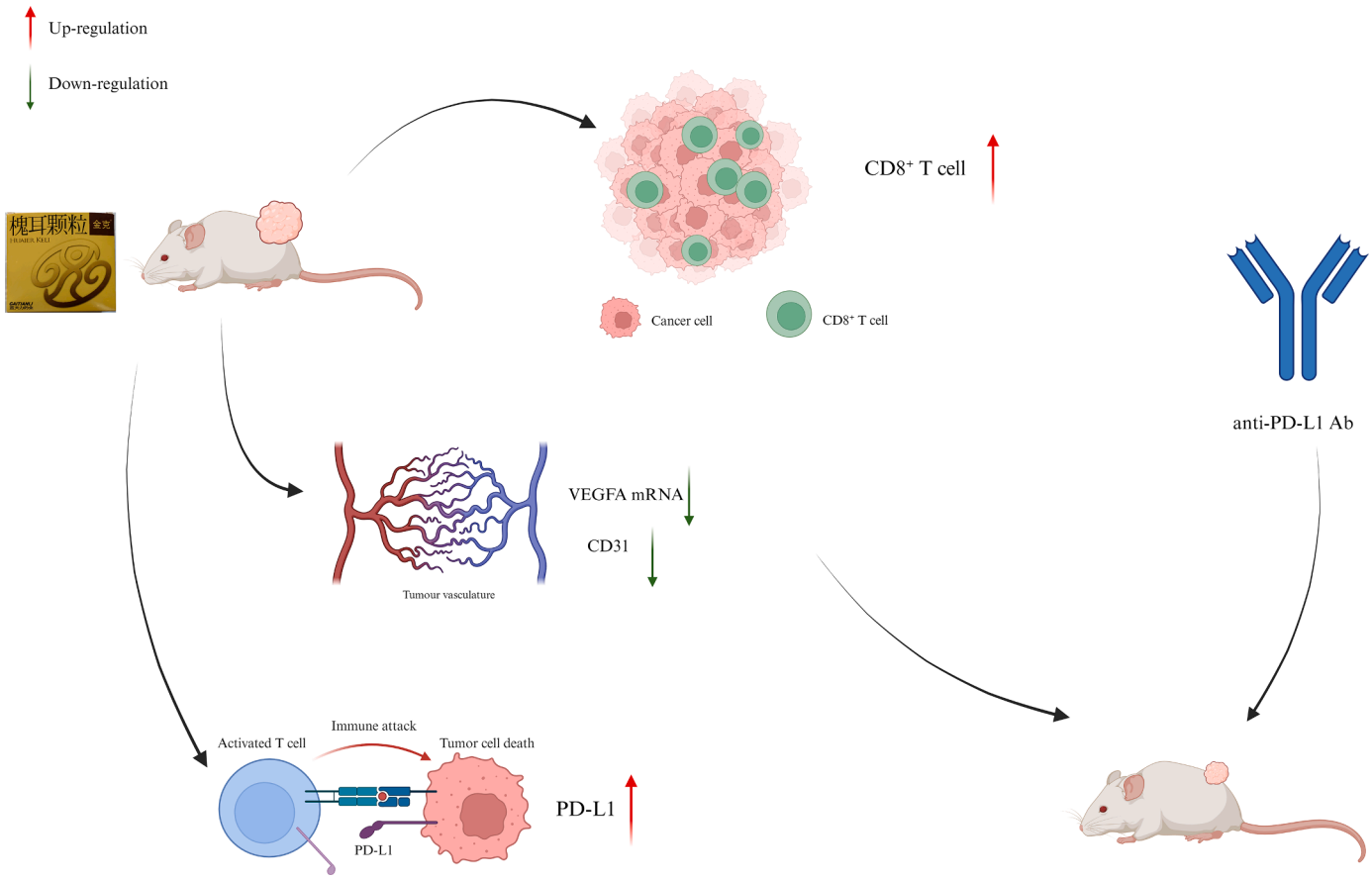

Fig. 9. Huaier had a modulating effect on the antitumor immune microenvironment. Huaier promoted the infiltration of $CD8^+$ T cells, downregulated the expression of VEGFA and CD31, and upregulated the expression of PD-L1. Huaier could improve the efficacy of anti-PD-L1 Ab in the treatment of HCC.

future research directions.

Conclusion

In this study, Huaier inhibited the growth of H22-bearing mice and promoted the increase of $CD8^+$ T cells. The antitumor effect of Huaier was significantly inhibited when it was combined with anti-CD8α Ab, which indicated that $CD8^+$ T cells are critical for Huaier to exert its antitumor effect. Additionally, Huaier downregulated VEGFA expression, inhibited MVD, and upregulated PD-L1 expression. The Huaier and anti-PD-L1 Ab combination produced significant antitumor effects. Transcriptome sequencing revealed that the action mechanism of this combination was strongly related to the immunomodulation and immune response induced by Huaier. The study results suggest that Huaier combined with anti-PD-L1 Ab is a safe and effective new modality for HCC treatment and that this combination regimen could be investigated in prospective or retrospective clinical trials to assess its clinical efficacy and promote the use of this regimen.

CRedit authorship contribution statement

Cheng Yi, Xi Yang, and Huawei Li designed the study. Huawei Li, Jia You, Yufeng Wei, Lingnan Zheng, Ju Yang, Jingyi Xu, Yue Li, and ZhaoJun Li performed the experiments. Cheng Yi and Xi Yang supervised the experiments. Huawei Li, Jia You, and Yufeng Wei processed the data. Huawei Li and Jia You drafted the draft. Huawei Li, You Jia, Wei Yufeng, Ju Yang, and Zhaojun Li revise this manuscript. All data were generated in-house, and no paper mill was used. All authors agree to be accountable for all aspects of work ensuring integrity and accuracy.

Declaration of Competing Interest

We declare that we do not have any commercial or associative interest that represents a conflict of interest in connection with the work submitted.

Acknowledgments

This research was provided support from the Hubei Chen Xiaoping Science and Technology Development Foundation 2021 Special Fund (Project no: CXPJJH121001–2021069), National Natural Science Foundation of China (Project no: 82260490), Sichuan Provincial Nature Science Foundation (Project no: 2022NSFSC1379), Sichuan Science and Technology Programme (Project no: 2022YFSY0054), Natural Science Foundation of Hainan Province (Project no: 821QN394), Science and technology research project on novel coronavirus pneumonia outbreak, West China Hospital, Sichuan University (Project no: HX-2019-nCoV-069). In addition, the authors thank Hangzhou LC-Biotech, China, and Kangtai Medical Laboratory Service Hebei Co. for technical assistance with transcriptome sequencing and HPLC-MS/MS in this study.

Supplementary materials

Supplementary material associated with this article can be found, in the online version, at doi:10.1016/j.phymed.2023.155189.

References

Abou-Alfa, G.K., Chan, S.L., Kudo, M., Lau, G., Kelley, R.K., Furuse, J., Sukeepaisarnjaroen, W., Kang, Y., Dao, T.V., De Toni, E.N., Rimassa, L., Breder, V.V., Vasilyev, A., Heurgue, A., Tam, V., Mody, K., Thungappa, S.C., He, P., Negro, A., Sangro, B., 2022. Phase 3 randomized, open-label, multicenter study of

tremelimumab (T) and durvalumab (D) as first-line therapy in patients (pts) with unresectable hepatocellular carcinoma (uHCC): HIMALAYA. JCO 40, 379.
Ai, L., Xu, A., Xu, J., 2020. Roles of PD-1/PD-L1 pathway: signaling, cancer, and beyond. Adv. Exp. Med. Biol. 1248, 33–59.
Akhtar, M., Rashid, S., Al-Bozom, I.A., 2021. PD-L1 immunostaining: what pathologists need to know. Diagn. Pathol. 16, 94.
Alspach, E., Lussier, D.M., Schreiber, R.D., 2019. Interferon γ and Its Important Roles in Promoting and Inhibiting Spontaneous and Therapeutic Cancer Immunity. CSH Perspect. Biol. 11.
Chen, Q., Shu, C., Laurence, A.D., Chen, Y., Peng, B., Zhen, Z., Cai, J., Ding, Y., Li, L., Zhang, Y., Zheng, Q., Xu, G., Li, B., Zhou, W., Cai, S., Wang, X., Wen, H., Peng, X., Zhang, X., Dai, C., Bie, P., Xing, B., Fu, Z., Liu, L., Mu, Y., Zhang, L., Zhang, Q., Jiang, B., Qian, H., Wang, Y., Liu, J., Qin, X., Li, Q., Yin, P., Zhang, Z., Chen, X., 2018. Effect of Huaier granule on recurrence after curative resection of HCC: a multicentre, randomised clinical trial. Gut 67, 2006–2016.
Cheng, A., Qin, S., Ikeda, M., Galle, P.R., Ducreux, M., Kim, T., Lim, H.Y., Kudo, M., Breder, V., Merle, P., Kaseb, A.O., Li, D., Verret, W., Ma, N., Nicholas, A., Wang, Y., Li, L., Zhu, A.X., Finn, R.S., 2022. Updated efficacy and safety data from IMbrave150: atezolizumab plus bevacizumab vs. sorafenib for unresectable hepatocellular carcinoma. J. Hepatol. 76, 862–873.
Consortium, T.G.O., 2017. Expansion of the gene ontology knowledgebase and resources. Nucleic. Acids. Res. 45, D331–D338.
El-Khoueiry, A.B., Sangro, B., Yau, T., Crocenzi, T.S., Kudo, M., Hsu, C., Kim, T., Choo, S., Trojan, J., Welling, T.H., Meyer, T., Kang, Y., Yeo, W., Chopra, A., Anderson, J., Dela Cruz, C., Lang, L., Neely, J., Tang, H., Dastani, H.B., Melero, I., 2017. Nivolumab in patients with advanced hepatocellular carcinoma (CheckMate 040): an open-label, non-comparative, phase 1/2 dose escalation and expansion trial. Lancet North Am. Ed. 389, 2492–2502.
Franz, L., Alessandrini, L., Calvanese, L., Crosetta, G., Frigo, A.C., Marioni, G., 2021. Angiogenesis, programmed death ligand 1 (PD-L1) and immune microenvironment association in laryngeal carcinoma. Pathology (Phila) 53, 844–851.
Fridman, W.H., Pagès, F., Sautès-Fridman, C., Galon, J., 2012. The immune contexture in human tumours: impact on clinical outcome. Nat. Rev. Cancer 12, 298–306.
Han, H., Jain, A.D., Truica, M.I., Izquierdo-Ferrer, J., Anker, J.F., Lysy, B., Sagar, V., Luan, Y., Chalmers, Z.R., Unno, K., Mok, H., Vatapalli, R., Yoo, Y.A., Rodriguez, Y., Kandela, I., Parker, J.B., Chakravarti, D., Mishra, R.K., Schiltz, G.E., Abdulkadir, S. A., 2019. Small-molecule MYC inhibitors suppress tumor growth and enhance immunotherapy. Cancer Cell 36, 483–497.
Hu, Z., Yang, A., Fan, H., Wang, Y., Zhao, Y., Zha, X., Zhang, H., Tu, P., 2016. Huaier aqueous extract sensitizes cells to rapamycin and cisplatin through activating mTOR signaling. J. Ethnopharmacol. 186, 143–150.
Li, C., Wu, X., Zhang, H., Yang, G., Hao, M., Sheng, S., Sun, Y., Long, J., Hu, C., Sun, X., Li, L., Zheng, J., 2015a. A Huaier polysaccharide inhibits hepatocellular carcinoma growth and metastasis. Tumor. Biol. 36, 1739–1745.
Li, C., Wu, X., Zhang, H., Yang, G., Hao, M., Sheng, S., Sun, Y., Long, J., Hu, C., Sun, X., Li, L., Zheng, J., 2015b. A Huaier polysaccharide reduced metastasis of human hepatocellular carcinoma SMMC-7721 cells via modulating AUF-1 signaling pathway. Tumour Biol.: J. Int. Soc. Oncodevelopm. Biol. Med. 36, 6285–6293.
Long, H., Wu, Z., 2023. Immunoregulatory effects of Huaier (Trametes robiniophila Murr) and relevant clinical applications. Front. Immunol. 14, 1147098.
Melincovici, C.S., Boşca, A.B., Şuşman, S., Mărginean, M., Mihu, C., Istrate, M., Moldovan, I.M., Roman, A.L., Mihu, C.M., 2018. Vascular endothelial growth factor (VEGF) - key factor in normal and pathological angiogenesis. Rom. J. Morphol. Embryol. 59, 455–467.
Morita, M., Nishida, N., Sakai, K., Aoki, T., Chishina, H., Takita, M., Ida, H., Hagiwara, S., Minami, Y., Ueshima, K., Nishio, K., Kobayashi, Y., Kakimi, K., Kudo, M., 2021. Immunological microenvironment predicts the survival of the patients with hepatocellular carcinoma treated with Anti-PD-1 antibody. Liver Cancer 10, 380–393.
Narayanan, S., de Mores, A.R., Cohen, L., Anwar, M.M., Lazar, F., Hicklen, R., Lopez, G., Yang, P., Bruera, E., 2023. Medicinal mushroom supplements in cancer: a systematic review of clinical studies. Curr. Oncol. Rep. 25, 569–587.
Ott, P.A., Hodi, F.S., Kaufman, H.L., Wigginton, J.M., Wolchok, J.D., 2017. Combination immunotherapy: a road map. J. Immunother. Cancer 5, 16.
Qin, S., Chan, L.S., Gu, S., Bai, Y., Ren, Z., Lin, X., Chen, Z., Jia, W., Jin, Y., Guo, Y., Sultanbaev, A.V., Pazgan-Simon, M., Pisetska, M., Liang, X., Chen, C., Nie, Z., Wang, L., Cheng, A., Kaseb, A., Vogel, A., 2022a. Camrelizumab (C) plus rivoceranib (R) vs. sorafenib (S) as first-line therapy for unresectable hepatocellular carcinoma (uHCC): a randomized, phase III trial. Ann. Oncol. 33, S1401–S1402.
Qin, S., Kudo, M., Meyer, T., Finn, R.S., Vogel, A., Bai, Y., Guo, Y., Meng, Z., Zhang, T., Satoh, T., Hiraoka, A., Marino, D., Assenat, E., Wyrwicz, L., Calvo Campos, M., Hsing-Tao, K., Boisserie, F., Li, S., Chen, Y., Zhu, A.X., 2022b. Final analysis of RATIONALE-301: randomized, phase III study of tislelizumab versus sorafenib as first-line treatment for unresectable hepatocellular carcinoma. Ann. Oncol. 33, S1402–S1403.
Qin, S., Ren, Z., Meng, Z., Chen, Z., Chai, X., Xiong, J., Bai, Y., Yang, L., Zhu, H., Fang, W., Lin, X., Chen, X., Li, E., Wang, L., Chen, C., Zou, J., 2020. Camrelizumab in patients with previously treated advanced hepatocellular carcinoma: a multicentre, open-label, parallel-group, randomised, phase 2 trial. Lancet Oncol. 21, 571–580.
Ren, J., Zheng, C., Feng, G., Liang, H., Xia, X., Fang, J., Duan, X., Zhao, H., 2009. Inhibitory effect of extract of fungi of Huaier on hepatocellular carcinoma cells. J. Huazhong Univ. Sci. Technol. [Med. Sci.] 29, 198–201.
Shan, L., Li, Y., Jiang, H., Tao, Y., Qian, Z., Li, L., Cai, F., Ma, L., Yu, Y., 2017. Huaier restrains proliferative and migratory potential of hepatocellular carcinoma cells partially through decreased yes-associated Protein 1. J. Cancer 8, 4087–4097.
Su, Y., Luo, B., Lu, Y., Wang, D., Yan, J., Zheng, J., Xiao, J., Wang, Y., Xue, Z., Yin, J., Chen, P., Li, L., Zhao, Q., 2022. Anlotinib induces a T cell-inflamed tumor microenvironment by facilitating vessel normalization and enhances the efficacy of PD-1 checkpoint blockade in neuroblastoma. Clin. Cancer Res.: Off. J. Am. Assoc. Cancer Res. 28, 793–809.
Sun, Y., Sun, T., Wang, F., Zhang, J., Li, C., Chen, X., Li, Q., Sun, S., 2013. A polysaccharide from the fungi of Huaier exhibits anti-tumor potential and immunomodulatory effects. Carbohyd. Polym. 92, 577–582.
Sung, H., Ferlay, J., Siegel, R.L., Laversanne, M., Soerjomataram, I., Jemal, A., Bray, F., 2021. Global cancer statistics 2020: GLOBOCAN estimates of incidence and mortality worldwide for 36 cancers in 185 countries. CA A Cancer J. Clin. 71, 209–249.
Tao, Y., Shan, L., Xu, X., Jiang, H., Chen, R., Qian, Z., Yang, Z., Liang, B., Zhen, H., Cai, F., Yu, Y., Ma, L., 2018. Huaier augmented the chemotherapeutic sensitivity of oxaliplatin via downregulation of YAP in hepatocellular carcinoma. J. Cancer 9, 3962–3970.
Villanueva, A., 2019. Hepatocellular carcinoma. New Engl. J. Med. 380, 1450–1462.
Wang, X., Zhang, N., Huo, Q., Yang, Q., 2012. Anti-angiogenic and antitumor activities of Huaier aqueous extract. Oncol. Rep. 28, 1167–1175.
Wang, Z., Yu, X., Zhang, J., Cheng, Z., Han, Z., Liu, F., Dou, J., Kong, Y., Dong, X., Zhao, Q., Yu, J., Liang, P., Tang, W., 2021. Huaier granule prevents the recurrence of early-stage hepatocellular carcinoma after thermal ablation: a cohort study. J. Ethnopharmacol. 281, 114539.
Wei, Y., Wang, Y., Liu, N., Qi, R., Xu, Y., Li, K., Feng, Y., Shi, B., 2022. A FAK inhibitor boosts Anti-PD1 immunotherapy in a hepatocellular carcinoma mouse model. Front. Pharmacol. 12, 820446.
Weidner, N., Folkman, J., Pozza, F., Bevilacqua, P., Allred, E.N., Moore, D.H., Meli, S., Gasparini, G., 1992. Tumor angiogenesis: a new significant and independent prognostic indicator in early-stage breast carcinoma. J. Natl. Cancer Inst. 84, 1875–1887.
Wu, M., Huang, Q., Xie, Y., Wu, X., Ma, H., Zhang, Y., Xia, Y., 2022. Improvement of the anticancer efficacy of PD-1/PD-L1 blockade via combination therapy and PD-L1 regulation. J. Hematol. Oncol. 15, 24.
Xu, X., Wei, Q., Wang, K., Ling, Q., Xie, H., Zhou, L., Zheng, S., 2011. Anticancer effects of Huaier are associated with down-regulation of P53. Asian Pacif. J. Cancer Prevent.: APJCP 12, 2251–2254.
Yang, L., Song, Z., Wang, X., Yang, W., Wang, M., Liu, H., 2017. Huaier extract enhances the treatment efficacy of paclitaxel in breast cancer cells via the NF-κB/IκBα pathway. Oncol. Rep. 38, 3455–3464.
Yau, T., Kang, Y., Kim, T., El-Khoueiry, A.B., Santoro, A., Sangro, B., Melero, I., Kudo, M., Hou, M., Matilla, A., Tovoli, F., Knox, J.J., Ruth He, A., El-Rayes, B.F., Acosta-Rivera, M., Lim, H., Neely, J., Shen, Y., Wisniewski, T., Anderson, J., Hsu, C., 2020. Efficacy and safety of nivolumab plus ipilimumab in patients with advanced hepatocellular carcinoma previously treated with sorafenib. JAMA Oncol. 6, e204564.
Yau, T., Zagonel, V., Santoro, A., Acosta-Rivera, M., Choo, S.P., Matilla, A., He, A.R., Cubillo Gracian, A., El-Khoueiry, A.B., Sangro, B., Eldawy, T.E., Bruix, J., Frassineti, G.L., Vaccaro, G.M., Tschaika, M., Scheffold, C., Koopmans, P., Neely, J., Piscaglia, F., 2022. Nivolumab plus Cabozantinib with or without ipilimumab for advanced hepatocellular carcinoma: results from Cohort 6 of the CheckMate 040 trial. J. Clin. Oncol.: Off. J. Am. Soc. Clin. Oncol., JCO2200972
Zhao, S., Jiang, T., Li, X., Zhou, C., 2017. Combining anti-angiogenesis and immunotherapy enhances antitumor effect by promoting immune response in lung cancer. J. Thorac. Oncol. 12, S288.
Zhu, A.X., Finn, R.S., Edeline, J., Cattan, S., Ogasawara, S., Palmer, D., Verslype, C., Zagonel, V., Fartoux, L., Vogel, A., Sarker, D., Verset, G., Chan, S.L., Knox, J., Daniele, B., Webber, A.L., Ebbinghaus, S.W., Ma, J., Siegel, A.B., Cheng, A., Kudo, M., Alistar, A., Asselah, J., Blanc, J., Borbath, I., Cannon, T., Chung, K., Cohn, A., Cosgrove, D.P., Damjanov, N., Gupta, M., Karino, Y., Karwal, M., Kaubisch, A., Kelley, R., Van Laethem, J., Larson, T., Lee, J., Li, D., Manhas, A., Manji, G.A., Numata, K., Parsons, B., Paulson, A.S., Pinto, C., Ramirez, R., Ratnam, S., Rizell, M., Rosmorduc, O., Sada, Y., Sasaki, Y., Stal, P.I., Strasser, S., Trojan, J., Vaccaro, G., Van Vlierberghe, H., Weiss, A., Weiss, K., Yamashita, T., 2018. Pembrolizumab in patients with advanced hepatocellular carcinoma previously treated with sorafenib (KEYNOTE-224): a non-randomised, open-label phase 2 trial. Lancet Oncol. 19, 940–952.
Zou, Y., Xiong, H., Xiong, H., Lu, T., Zhu, F., Luo, Z., Yuan, X., Wang, Y., 2015. A polysaccharide from mushroom Huaier retards human hepatocellular carcinoma growth, angiogenesis, and metastasis in nude mice. Tumor. Biol. 36, 2929–2936.
Jianwu, J., Xiaolan, L.I., Yan, L., Deding, T., Junbo, H.U., Jianping, G., 2015. Effect of Huaier granules on invasion and metastasis of colorectal cancer SW480 cells in vitro. Herald Med. 34, 455–458.
Yang, J., Xiaoming, J., Kang, T., 2007. A primary study using the method of average positive stained area percentage to measure the immunohistochemistry results. J. Biomed. Eng. 24, 650–653.
Deng-xuan, M., Yang, Z., Yu-ping, L., Yan, C., 2023. Advances of immune-vascular crosstalk for oncology therapeutics. Chinese Pharmacol. Bull. 39, 212–218.
Xue-zheng, S., Zhen-hua, Z., Zhi-kun, H., Xin, Z., Hui-jiang, S., Guan-fu, T., Hong, F., Pei-tu, R., 2013. Effects of Huaier granules combined with TACE on T lymphocyte subsets in patients with advanced liver cancer. Chinese J. Tradit. Med. Sci. Technol. 20, 66.
Zheng-guang, Z., Bing, L., Wei-feng, L., Cun-si, S., 2020. Preliminary study on reversal of sorafenib resistance of hepatocellular carcinoma cells by Huaier granule. J. Nanjing Univ. Tradit. Chinese Med. 36, 83–87.

Positive Mode

Name	Formula	CAS_num	Class	Annot. DeltaMass [ppm]	Annotation MW	Calc. MW	RT [min]	Area	Relative concentrations of components in Huaier (μg/ml)	Relative percentage of constituents in Huaier (%)
5'-S-Methyl-5'-thioadenosine	C11 H15 N5 O3 S	2457-80-9	5'-deoxyribonucleosides	-4.12	297.08956	297.08833	4.28	148951804.7	0.103140819	0.153%
Ecgonine	C9 H15 N O3	481-37-8	Tropane alkaloids	-3.83	185.10519	185.10448	1.099	78087968.53	0.054071564	0.080%
Ecgonine methyl ester	C10 H17 N O3	7143/9/1	Tropane alkaloids	-3.25	199.12084	199.1202	7.245	19921438.81	0.013794486	0.021%
DIBOA	C8 H7 N O4	17359-54-5	Benzoxazines	-2.7	181.03751	181.03702	2.275	34654281.27	0.023996157	0.036%
1-(1H-Benzo[d]imidazol-2-yl)ethan-1-ol	C9 H10 N2 O	NA	Benzimidazoles	-2.89	162.07931	162.07884	1.753	61980285.14	0.042917891	0.064%
Ancymidol	C15 H16 N2 O2	12771-68-5	Phenol ethers	-4.55	256.12118	256.12001	7.771	4490050.482	0.00310911	0.005%
Penbutolol	C18 H29 N O2	36507-48-9	Phenol ethers	-4.8	291.21983	291.21843	8.778	18537631.65	0.012836276	0.019%
Styrene	C8 H8	100-42-5	Benzene and substituted derivatives	-0.34	104.0626	104.06256	3.05	307637723.4	0.213021969	0.317%
Chlorobenzene	C6 H5 Cl	108-90-7	Benzene and substituted derivatives	-4.31	112.00798	112.0075	4.251	2615167804	1.810857881	2.691%
Sulfanilic acid	C6 H7 N O3 S	121-57-3	Benzene and substituted derivatives	-2.77	173.01466	173.01419	3.453	22180937.87	0.015359063	0.023%
4-Methoxybenzaldehyde	C8 H8 O2	123-11-5	Benzene and substituted derivatives	-3.02	136.05243	136.05202	6.452	36651354.86	0.02537902	0.038%
4-Amino-3-hydroxybenzoic acid	C7 H7 N O3	2374-03-0	Benzene and substituted derivatives	-2.59	153.04259	153.0422	3.808	68369196.65	0.047341856	0.070%
N-(2,4-Dimethylphenyl)-N'-methylimidoformamide	C10 H14 N2	33089-74-6	Benzene and substituted derivatives	-3.23	162.1157	162.11518	4.438	87950252.8	0.060900646	0.091%
Tolycaine	C15 H22 N2 O3	3686-58-6	Benzene and substituted derivatives	-3.73	278.16304	278.162	6.202	132198576.8	0.091540143	0.136%
Norneosildenafil	C22 H29 N5 O4 S	371959-09-0	Benzene and substituted derivatives	-1.08	459.19402	459.19353	0.887	376837035.1	0.260938634	0.388%
Methyl-3-aminobenzoate	C8 H9 N O2	4518/10/9	Benzene and substituted derivatives	-2.95	151.06333	151.06288	6.556	83298400.02	0.057679497	0.086%
Syringic acid	C9 H10 O5	530-57-4	Benzene and substituted derivatives	-3.08	198.05282	198.05221	5.762	21590208.99	0.014950016	0.022%
Phenylacetylene	C8 H6	536-74-3	Benzene and substituted derivatives	-1.6	102.04695	102.04679	2.032	3415659791	2.365153945	3.515%
Neostigmine	C12 H18 N2 O2	59-99-4	Benzene and substituted derivatives	-3.37	222.13683	222.13608	6.045	32996239.97	0.022848056	0.034%
Benzamidine	C7 H8 N2	618-39-3	Benzene and substituted derivatives	-1.38	120.06875	120.06858	2.256	28935214.21	0.020036022	0.030%
Phenacetin	C10 H13 N O2	62-44-2	Benzene and substituted derivatives	-4.04	179.09463	179.0939	7.63	10845059.07	0.007509599	0.011%
N-Benzylformamide	C8 H9 N O	6343-54-0	Benzene and substituted derivatives	-2.99	135.06841	135.06801	5.648	41876395.14	0.028997069	0.043%
Benzoic acid	C7 H6 O2	65-85-0	Benzene and substituted derivatives	-1.16	122.03678	122.03664	1.18	64116766.87	0.044397286	0.066%
Fenpropimorph	C20 H33 N O	67564-91-4	Benzene and substituted derivatives	-4.84	303.25621	303.25475	8.079	13720466.15	0.009500658	0.014%
Detomidine	C12 H14 N2	76631-46-4	Benzene and substituted derivatives	-2.89	186.1157	186.11516	5.789	17564174.01	0.012162211	0.018%
Isovanillic acid	C8 H8 O4	NA	Benzene and substituted derivatives	-3.36	168.04226	168.04169	5.591	30185991.04	0.020902116	0.031%

2,6-Diaminotoluene	C7 H10 N2	823-40-5	Benzene and substituted derivatives	-1.69	122.0844	122.08419	1.616	53655096.98	0.037153163	0.055%
L(-)-2-Amino-3-phenyl-1-propanol	C9 H13 N O	3182-95-4	Benzene and substituted derivatives	-3.51	151.09971	151.09918	10.811	3723743.793	0.002578485	0.004%
2-Pyridylacetic acid	C7 H7 N O2	13115-43-0	Pyridines and derivatives	-3.18	137.04768	137.04724	4.884	31598400.96	0.021880131	0.033%
Nicotinic acid 1-oxide	C6 H5 N O3	2398-81-4	Pyridines and derivatives	-2.73	139.02694	139.02656	1.106	435611115.4	0.301636407	0.448%
Methyl isonicotinate	C7 H7 N O2	2459-09-8	Pyridines and derivatives	-3.18	137.04768	137.04724	0.902	286112762	0.198117134	0.294%
Pirbuterol	C12 H20 N2 O3	38677-81-5	Pyridines and derivatives	-3.65	240.14739	240.14652	1.399	429147436.2	0.29716067	0.442%
1-Butylpyridinium	C9 H13 N	45806-95-9	Pyridines and derivatives	-2.82	135.1048	135.10442	5.164	9820230.051	0.006799962	0.010%
Cotinine	C10 H12 N2 O	486-56-6	Pyridines and derivatives	-3.24	176.09496	176.09439	6.019	25186216.29	0.01744005	0.026%
2-Methylnicotinamide	C7 H8 N2 O	58539-65-4	Pyridines and derivatives	-2.7	136.06366	136.0633	3.531	34829645.81	0.024117588	0.036%
Pyridoxal	C8 H9 N O3	66-72-8	Pyridines and derivatives	-4.1	167.05824	167.05756	8.7	10090593.08	0.006987173	0.010%
Pyridoxamine	C8 H12 N2 O2	85-87-0	Pyridines and derivatives	-2.82	168.08988	168.0894	2.233	383035767.3	0.265230911	0.394%
Nicotinamide	C6 H6 N2 O	98-92-0	Pyridines and derivatives	-1.74	122.04801	122.0478	3.065	58212803.41	0.04030912	0.060%
6-Hydroxynicotinic acid	C6 H5 N O3	5006-66-6	Pyridines and derivatives	-2.79	139.02694	139.02655	1.432	1054518143	0.730195014	1.085%
N-ethylmaleimide	C6 H7 N O2	128-53-0	Pyrrolidines	-1.71	125.04768	125.04746	1.877	305177722.1	0.211318556	0.314%
Anhydroecgonine methyl ester	C10 H15 N O2	43021-26-7	Pyrrolidines	-3.21	181.11028	181.1097	8.905	10837027.77	0.007504037	0.011%
N-Hydroxysuccinimide	C4 H5 N O3	6066-82-6	Pyrrolidines	-4.06	115.02694	115.02648	0.902	300869611.9	0.20833543	0.310%
1,5-Ditetrahydro-1H-pyrrol-1-ylpentane-1,5-dione	C13 H22 N2 O2	NA	Pyrrolidines	-4.63	238.16813	238.16702	8.389	6539623.05	0.004528324	0.007%
1,3-Divinyl-2-imidazolidinone	C7 H10 N2 O	13811-50-2	Azolidines	-3.47	138.07931	138.07883	3.812	77505421.28	0.053668182	0.080%
2-Morpholino-5-(1H-pyrrol-1-yl)benzoic acid	C15 H16 N2 O3	690632-76-9	Oxazinanes	-3.76	272.11609	272.11507	5.791	33391230.92	0.023121565	0.034%
Tridemorph	C19 H39 N O	81412-43-3	Oxazinanes	-3.24	297.30316	297.3022	19.029	15670310.75	0.010850816	0.016%
1-(2-Morpholinophenyl)dihydro-1H-pyrrole-2,5-dione	C14 H16 N2 O3	NA	Oxazinanes	-3.35	260.11609	260.11522	4.953	61516084.09	0.042596458	0.063%
Vasicinone	C11 H10 N2 O2	486-64-6	Diazanaphthalenes	-3.51	202.07423	202.07352	5.349	16599687.99	0.011494358	0.017%
Quinoxalinedione + 2Methyl + C5H11O4	C15 H20 N2 O6	NA	Diazanaphthalenes	-3.64	324.13214	324.13096	5.726	38486107.56	0.026649483	0.040%
Linderane	C15 H16 O4	13476-25-0	Dioxanes	-3.57	260.10486	260.10393	6.873	14602224.76	0.010111226	0.015%
Bis(4-ethylbenzylidene)sorbitol	C24 H30 O6	79072-96-1	Dioxanes	-4.29	414.20424	414.20246	11.852	36267014.19	0.025112885	0.037%
3,3-Dimethyl-1,2-dithiolane	C5 H10 S2	58384-57-9	Dithiolanes	0.22	134.02239	134.02242	1.267	653071150.6	0.452215356	0.672%
4,6-Dimethyl-2(1H)-pyrimidinone	C6 H8 N2 O	108-79-2	Diazines	-2.29	124.06366	124.06338	2.132	64435906.4	0.044618272	0.066%
Methohexital	C14 H18 N2 O3	151-83-7	Diazines	-3.54	262.13174	262.13082	5.665	51788019.71	0.035860316	0.053%
Dihydrothymine	C5 H8 N2 O2	19140-80-8	Diazines	-3.01	128.05858	128.05819	0.815	329879307.2	0.228423026	0.339%
Cytosine	C4 H5 N3 O	71-30-7	Diazines	-0.12	111.04326	111.04325	1.071	72802926.17	0.050411967	0.075%
2-sec-Butyl-3-methoxypyrazin	C9 H14 N2 O	NA	Diazines	-3.03	166.11061	166.11011	2.764	24073347.91	0.016669451	0.025%
1-Phenylhexahydropyridazine-3,6-dione	C10 H10 N2 O2	NA	Diazinanes	-3.75	190.07423	190.07351	2.763	72082087.71	0.049912826	0.074%
Phloroglucinol	C6 H6 O3	108-73-6	Phenols	-2.06	126.03169	126.03143	3.547	292159535.6	0.202304187	0.301%
Vanillin	C8 H8 O3	121-33-5	Phenols	-3.41	152.04734	152.04683	6.498	23560904.7	0.016314613	0.024%
Epinephrine	C9 H13 N O3	51-43-4	Phenols	-2.85	183.08954	183.08902	2.797	24222540.45	0.016772759	0.025%
Phenylephrine	C9 H13 N O2	59-42-7	Phenols	-4.06	167.09463	167.09395	9.217	8266987.21	0.005724428	0.009%
Betaxolol	C18 H29 N O3	63659-18-7	Phenols	-4.29	307.21474	307.21343	8.612	97346658.33	0.067407133	0.100%
Salicylamide	C7 H7 N O2	65-45-2	Phenols	-2.73	137.04768	137.0473	2.262	88495517.1	0.061278211	0.091%
5-{8(Z),11(Z)-pentadecadienyl}resorcinol	C21 H32 O2	79473-25-9	Phenols	-4.18	316.24023	316.23891	10.529	35407447.88	0.024517683	0.036%
2-Furoic acid	C5 H4 O3	88-14-2	Furans	-0.45	112.01604	112.01599	3.645	67919285.75	0.047030318	0.070%
PC(16:0/0:0)	C24 H50 N O7 P	17364-16-8	Glycerophospholipids	-3.79	495.33249	495.33061	12.817	66514466.36	0.046057559	0.068%
LPC 18:1	C26 H52 N O7 P	19420-56-5	Glycerophospholipids	-3.53	521.34814	521.3463	13.163	11230316.21	0.007776368	0.012%
LPC 18:2	C26 H50 N O7 P	22252-07-9	Glycerophospholipids	-3.41	519.33249	519.33072	12.343	189006004.6	0.130876119	0.194%
LPE 18:2	C23 H44 N O7 P	85046-18-0	Glycerophospholipids	-3.71	477.28554	477.28377	12.176	11892666.89	0.008235009	0.012%
1-Stearoylglycerol	C21 H42 O4	123-94-4	Glycerolipids	-3.73	358.30831	358.30697	18.905	25871577.48	0.017914625	0.027%
5-Hydroxy-2',4',7,8-Tetramethoxyflavone	C19 H18 O7	123316-61-0	Flavonoids	-3.87	358.10525	358.10387	11.613	4953602.822	0.003430094	0.005%
Nobiletin	C21 H22 O8	478-01-3	Flavonoids	-3.83	402.13147	402.12993	11.088	248471609.7	0.172052735	0.256%
Tangeritin	C20 H20 O7	481-53-8	Flavonoids	-3.79	372.1209	372.11949	11.606	197643304	0.136856967	0.203%
Corymboside	C26 H28 O14	73543-87-0	Flavonoids	-2.98	564.14791	564.14623	6.011	114855726.5	0.079531186	0.118%

NCGC00384563-02!5,7-dihydroxy-2-(4-hydroxyphenyl)-6,8-bis(3,4,5-trihydroxyoxan-2-yl)chromen-4-one	C25 H26 O13	NA	Flavonoids	-3.25	534.13734	534.13561	6.369	19837058.88	0.013736057	0.020%
6-Quinolinecarboxylic acid	C10 H7 N O2	10349-57-2	Quinolines and derivatives	-2.52	173.04768	173.04724	1.345	61313480.16	0.042456166	0.063%
8-Hydroxyquinoline	C9 H7 N O	148-24-3	Quinolines and derivatives	-2.72	145.05276	145.05237	4.506	198087464.8	0.137164524	0.204%
Kynurenic acid	C10 H7 N O3	492-27-3	Quinolines and derivatives	-3.01	189.04259	189.04202	4.557	89441790.29	0.061933452	0.092%
2-Hydroxyquinoline	C9 H7 N O	59-31-4	Quinolines and derivatives	-2.93	145.05276	145.05234	3.819	65040789.5	0.04503712	0.067%
Primobolan	C27 H42 O3	303-42-4	Steroids and steroid derivatives	-4.55	414.3134	414.31151	10.125	10004745.87	0.006927729	0.010%
Medroxyprogesterone	C22 H32 O3	520-85-4	Steroids and steroid derivatives	-3.96	344.23514	344.23378	11.093	3870462.335	0.002680079	0.004%
Testosterone cypionate	C27 H40 O3	58-20-8	Steroids and steroid derivatives	-4.36	412.29775	412.29595	8.954	3232911.961	0.002238611	0.003%
Testosterone	C19 H28 O2	58-22-0	Steroids and steroid derivatives	-4.31	288.20893	288.20769	10.533	18995782.82	0.01315352	0.020%
Ergosterol peroxide	C28 H44 O3	2061-64-5	Steroids and steroid derivatives	-4.81	428.32905	428.32698	9.7	9337100.118	0.006465421	0.010%
Kahweol	C20 H26 O3	6894-43-5	Naphthofurans	-3.45	314.18819	314.18711	7.181	19466037.36	0.013479145	0.020%
3-(2-Naphthyl)-L-alanine	C13 H13 N O2	6960-34-5	Naphthalenes	-3.9	215.09463	215.09379	10.039	14309078.81	0.009908239	0.015%
2-Naphthylamine	C10 H9 N	91-59-8	Naphthalenes	-3.19	143.0735	143.07304	5.306	87850757.31	0.060831751	0.090%
delta-Decalactone	C10 H18 O2	705-86-2	Lactones	-4.37	170.13068	170.12994	8.808	17772975.48	0.012306794	0.018%
3-HYDROXY-4-(SUCCIN-2-YL)-CARYOLANE delta-LACTONE	C19 H28 O4	NA	Lactones	-4.99	320.19876	320.19716	8.158	3492988.777	0.0024187	0.004%
Azobenzene	C12 H10 N2	103-33-3	Azobenzenes	-2.68	182.0844	182.08391	6.085	53108985.58	0.036775011	0.055%
Guanosine	C10 H13 N5 O5	118-00-3	Purine nucleosides	-3.59	283.09167	283.09065	1.266	344709083.2	0.238691819	0.355%
N6-Threonylcarbamoyladenosine	C15 H20 N6 O8	24719-82-2	Purine nucleosides	-3.62	412.13426	412.13277	4.93	13923642.49	0.009641346	0.014%
Adenosine	C10 H13 N5 O4	58-61-7	Purine nucleosides	-3.41	267.09675	267.09584	4.805	10533030.83	0.007293537	0.011%
N6-Me-Adenosine	C11 H15 N5 O4	60209-41-8	Purine nucleosides	-2.9	281.1124	281.11159	1.775	31982289.7	0.022145952	0.033%
Adenosine 5'-monophosphate	C10 H14 N5 O7 P	61-19-8	Purine nucleotides	-3.57	347.06308	347.06185	1.092	355385665.2	0.246084757	0.366%
N-(4-Hydroxy-3-nitrophenyl)-2-[(1-methyl-2,4,6-trioxohexahydro-5-pyrimidinyl)carbonyl]hydrazinecarboxamide	C13 H12 N6 O8	NA	others	-2.7	380.07166	380.07063	0.782	2188497989 0	15.15412825	22.521%
N-Benzyloxycarbonylglycine	C10 H11 N O4	1138-80-3	Others	-3.14	209.06881	209.06815	1.698	54115771.26	0.037472154	0.056%
Aurantiamide	C25 H26 N2 O3	58115-31-4	Others	-4.21	402.19434	402.19265	10.814	24582393.45	0.017021937	0.025%
NCGC00347762-02!3-benzyl-6-(1H-indol-3-ylmethyl)piperazine-2,5-dione	C20 H19 N3 O2	82597-82-8	Others	-4.5	333.14773	333.14623	8.578	16315986.66	0.011297911	0.017%
Stearidonoyl glycine	C20 H31 N O3	NA	Others	-3.75	333.23039	333.22914	5.028	20456391.65	0.014164911	0.021%
2-Methoxy-N-[(3S,3aS,8S,9S,9aS,9bS)-3,5a,9-trimethyl-2-oxododecahydronaphtho[1,2-b]furan-8-yl]acetamide	C18 H29 N O4	NA	Others	-3.73	323.20966	323.20845	6.577	8722273.161	0.006039688	0.009%
15-Deoxy-Δ12,14-prostaglandin A1	C20 H30 O3	NA	Others	-4.27	318.21949	318.21813	7.806	16025566.9	0.011096811	0.016%
Ethyl 2-amino-4-methyl-5-pyrimidinecarboxylate	C8 H11 N3 O2	NA	Others	-2.67	181.08513	181.08464	1.598	286636076.8	0.1984795	0.295%
4-{1-[1-(2-Methoxyethyl)-1H-tetrazol-5-yl]-2-methylpropyl}morpholine	C12 H23 N5 O2	NA	Others	-3.54	269.18517	269.18422	3.51	348464223	0.241292044	0.359%
1-{4-[(3-{[5-(2-Hydroxy-2-propanyl)-1,2-oxazol-3-yl]methyl}-3-oxetanyl)amino]-1-piperidinyl}ethanone	C17 H27 N3 O4	NA	Others	-3.63	337.20016	337.19893	6.46	13890292.58	0.009618253	0.014%
1,8-Diazabicyclo [5.4.0]undec-7-ene	C9 H16 N2	6674-22-2	Azepanes	-2.88	152.13135	152.13091	4.545	18456681.46	0.012780223	0.019%
p-Coumaraldehyde	C9 H8 O2	20711-53-9	Cinnamaldehydes	-3.36	148.05243	148.05193	2.037	4270926795	2.957378656	4.395%
Diferuloyl putrescine	C24 H28 N2 O6	42369-86-8	Cinnamic acids and derivatives	-3.85	440.19474	440.19304	8.254	25750095.11	0.017830505	0.026%
Ferulic acid	C10 H10 O4	537-98-4	Cinnamic acids and derivatives	-2.89	194.05791	194.05735	6.835	48089233.08	0.033299112	0.049%
2-Hydroxycinnamic acid	C9 H8 O3	614-60-8	Cinnamic acids and derivatives	-2.44	164.04734	164.04694	1.181	697311233.6	0.482849147	0.718%
Dicoumaroyl Spermidine	C25 H31 N3 O4	65715-79-9	Cinnamic acids and derivatives	-3.62	437.23146	437.22988	6.364	83558896.45	0.057859876	0.086%
4-Coumaric acid	C9 H8 O3	7400-08-0	Cinnamic acids and	-2.27	164.04734	164.04697	6.285	503700909.2	0.348784793	0.518%

			derivatives							
N1-(3-Pyridylmethyl)-3-(3,4-dichlorophenyl)acrylamide	C15 H12 Cl2 N2 O	NA	Cinnamic acids and derivatives	4.6	306.03267	306.03407	0.845	233423949.8	0.161633069	0.240%
2-Isopropyl-5-thieno[3,2-b]thiophen-2-yl-1,3,4-oxadiazole	C11 H10 N2 O S2	NA	Thienothiophenes	-3.54	250.02345	250.02257	0.705	25947274.1	0.01796704	0.027%
Atrazine	C8 H14 Cl N5	1912-24-9	Triazines	0.75	215.09377	215.09393	5.513	54863873.02	0.037990173	0.056%
Pilocarpine	C11 H16 N2 O2	54-71-7	Alkaloids and derivatives	-2.96	208.12118	208.12056	5.621	49154126.43	0.034036492	0.051%
D-1,2,3,4-Tetrahydroisoquinoline-3-carboxylic acid	C10 H11 N O2	74163-81-8	Tetrahydroisoquinolines	-3.17	177.07898	177.07842	2.296	66797797.16	0.04625375	0.069%
Stearamide	C18 H37 N O	124-26-5	Carboximidic acids and derivatives	-4.06	283.28751	283.28636	18.845	309144464.9	0.214065304	0.318%
Levetiracetam	C8 H14 N2 O2	102767-28-2	Carboxylic acids and derivatives	-2.97	170.10553	170.10502	4.512	39632499.75	0.027443296	0.041%
3-oxo-C4-homoserine lactone	C8 H11 N O4	106983-29-3	Carboxylic acids and derivatives	-2.41	185.06881	185.06836	1.449	92516440.82	0.064062476	0.095%
Betaine	C5 H11 N O2	107-43-7	Carboxylic acids and derivatives	-1.85	117.07898	117.07876	0.805	20778392708	14.38787833	21.382%
Fumonisin B1	C34 H59 N O15	116355-83-0	Carboxylic acids and derivatives	-3.88	721.38847	721.38567	8.926	12594264.87	0.008720826	0.013%
Cyclo(phenylalanyl-prolyl)	C14 H16 N2 O2	14705-60-3	Carboxylic acids and derivatives	-3.09	244.12118	244.12042	6.795	189379833.7	0.131134975	0.195%
L-Phenylalanine	C9 H11 N O2	150-30-1	Carboxylic acids and derivatives	-2.94	165.07898	165.07849	6.172	29633096.64	0.020519267	0.030%
N6,N6,N6-Trimethyl-L-lysine	C9 H20 N2 O2	19253-88-4	Carboxylic acids and derivatives	-3.81	188.15248	188.15176	0.758	604642717.5	0.418681366	0.622%
2-Aminooctanedioic acid	C8 H15 N O4	19641-59-9	Carboxylic acids and derivatives	-2.79	189.10011	189.09958	1.291	75758432.82	0.05245849	0.078%
N-Acetyl-L-tyrosine	C11 H13 N O4	19764-32-0	Carboxylic acids and derivatives	-3.48	223.08446	223.08368	2.294	144497275.8	0.100056306	0.149%
N-Acetylarginine	C8 H16 N4 O3	210545-23-6	Carboxylic acids and derivatives	-1.26	216.12224	216.12197	1.088	37259273.17	0.025799969	0.038%
E-N-Deoxyfructosyllysine	C12 H24 N2 O7	21291-40-7	Carboxylic acids and derivatives	-3.45	308.15835	308.15729	0.682	31045617.18	0.021497359	0.032%
Aspartame	C14 H18 N2 O5	22839-47-0	Carboxylic acids and derivatives	-3.23	294.12157	294.12062	2.238	72965072.78	0.050524244	0.075%
Phenylalanylisoleucine (isomer of 1329)	C15 H22 N2 O3	22951-94-6	Carboxylic acids and derivatives	-3.84	278.16304	278.16197	5.76	38630868.26	0.026749722	0.040%
Argininosuccinic acid	C10 H18 N4 O6	2387-71-5	Carboxylic acids and derivatives	-4.06	290.12263	290.12146	0.836	179076265.4	0.124000328	0.184%
Leucylleucine	C12 H24 N2 O3	2883-36-5	Carboxylic acids and derivatives	-3.29	244.17869	244.17789	5.605	202157884.6	0.139983063	0.208%
Ala-Ile	C9 H18 N2 O3	29727-65-9	Carboxylic acids and derivatives	-2.85	202.13174	202.13117	2.615	140005235.4	0.096945819	0.144%
Ala-Phe	C12 H16 N2 O3	3061-90-3	Carboxylic acids and derivatives	-3.75	236.11609	236.11521	2.607	44885332.4	0.03108059	0.046%
Glu-Val-Phe	C19 H27 N3 O6	31461-61-7	Carboxylic acids and derivatives	-3.95	393.18999	393.18843	5.89	8364895.954	0.005792224	0.009%
L-Norleucine	C6 H13 N O2	327-56-0	Carboxylic acids and derivatives	-3.08	131.09463	131.09422	5.552	31840299.13	0.022047632	0.033%
D-(+)-Proline	C5 H9 N O2	344-25-2	Carboxylic acids and derivatives	-1.21	115.06333	115.06319	0.814	398726529.9	0.276095889	0.410%
Phenylalanylvaline	C14 H20 N2 O3	3918-90-9	Carboxylic acids and derivatives	-3.66	264.14739	264.14643	4.893	80439765.61	0.055700052	0.083%

Valylvaline	C10 H20 N2 O3	3918-94-3	Carboxylic acids and derivatives	-3.2	216.14739	216.1467	1.608	100639716.1	0.069687392	0.104%
DL-Stachydrine	C7 H13 N O2	4136-37-2	Carboxylic acids and derivatives	-3.35	143.09463	143.09415	0.823	701415779.4	0.485691316	0.722%
4-Guanidinobutyric acid	C5 H11 N3 O2	463-00-3	Carboxylic acids and derivatives	-3.02	145.08513	145.08469	1.088	190381729.4	0.131828732	0.196%
Kainic acid	C10 H15 N O4	487-79-6	Carboxylic acids and derivatives	-3.92	213.10011	213.09927	5.55	36165019.51	0.025042259	0.037%
L-Ergothioneine	C9 H15 N3 O2 S	497-30-3	Carboxylic acids and derivatives	-3.37	229.0885	229.08772	0.845	186691059.5	0.129273149	0.192%
L-Histidine	C6 H9 N3 O2	4998-57-6	Carboxylic acids and derivatives	-2.73	155.06948	155.06905	0.699	30252176.93	0.020947946	0.031%
Threonylleucine (isomer of 809, 926)	C10 H20 N2 O4	50299-12-2	Carboxylic acids and derivatives	-3.29	232.14231	232.14154	2.246	42162157.63	0.029194943	0.043%
DL-Pipecolinic acid	C6 H11 N O2	535-75-1	Carboxylic acids and derivatives	-2.16	129.07898	129.0787	1.509	148534080.9	0.102851569	0.153%
Cyclo(leucylprolyl)	C11 H18 N2 O2	5654-86-4	Carboxylic acids and derivatives	-3.56	210.13683	210.13608	6.364	315071394.3	0.218169372	0.324%
NCGC00381364-01!3-propan-2-yl-2,3,6,7,8,8a-hexahydropyrrolo[1,2-a]pyrazine-1,4-dione	C10 H16 N2 O2	5654-87-5	Carboxylic acids and derivatives	-2.91	196.12118	196.12061	5.024	271976315.5	0.188328433	0.280%
Creatine	C4 H9 N3 O2	57-00-1	Carboxylic acids and derivatives	-2.7	131.06948	131.06912	0.824	25257811.72	0.017489626	0.026%
Prolylleucine	C11 H20 N2 O3	61596-47-2	Carboxylic acids and derivatives	-2.97	228.14739	228.14672	1.32	1907086180	1.320550839	1.962%
Crotetamide	C12 H22 N2 O2	6168-76-9	Carboxylic acids and derivatives	-4.34	226.16813	226.16715	7.795	67653754.88	0.046846453	0.070%
Leucylproline	C11 H20 N2 O3	6403-35-6	Carboxylic acids and derivatives	-3.24	228.14739	228.14665	4.2	102582379.9	0.071032578	0.106%
Serylleucine	C9 H18 N2 O4	6665-16-3	Carboxylic acids and derivatives	-3.41	218.12666	218.12591	2.322	74269134.32	0.051427234	0.076%
DL-Lysine	C6 H14 N2 O2	70-54-2	Carboxylic acids and derivatives	-2.59	146.10553	146.10515	0.684	162840571.6	0.112758016	0.168%
Leucylvaline	C11 H22 N2 O3	72121-02-9	Carboxylic acids and derivatives	-3.25	230.16304	230.16229	4.438	229811228.2	0.159131461	0.236%
Cyclo(phenylalanylleucyl), (3S,6S)-form	C15 H20 N2 O2	7280-77-5	Carboxylic acids and derivatives	-4.2	260.15248	260.15138	8.1	61343081.34	0.042476663	0.063%
NCGC00380373-01!2-[(2-amino-3-methylbutanoyl)amino]-3-phenylpropanoic acid	C14 H20 N2 O3	75946-40-6	Carboxylic acids and derivatives	-3.84	264.14739	264.14638	5.273	114526928.8	0.079303512	0.118%
Glycyl-L-leucine	C8 H16 N2 O3	869-19-2	Carboxylic acids and derivatives	-2.77	188.11609	188.11557	1.493	66491012.83	0.046041319	0.068%
tert-Butyl N-[1-(aminocarbonyl)-3-methylbutyl]carbamate	C11 H22 N2 O3	96928-99-3	Carboxylic acids and derivatives	-3.32	230.16304	230.16228	3.749	182781995.9	0.12656634	0.188%
Cyclo-prolylglycine	C7 H10 N2 O2	97011-16-0	Carboxylic acids and derivatives	-3.31	154.07423	154.07372	2.041	80596169.95	0.055808354	0.083%
L-Pyroglutamic acid	C5 H7 N O3	98-79-3	Carboxylic acids and derivatives	-1.9	129.04259	129.04235	1.134	1866391576	1.292372095	1.921%
α-Aspartylphenylalanine	C13 H16 N2 O5	NA	Carboxylic acids and derivatives	-3.73	280.10592	280.10488	1.829	70984567.14	0.049152855	0.073%
L-Isoleucine	C6 H13 N O2	NA	Carboxylic acids and derivatives	-2.15	131.09463	131.09435	1.31	5769685246	3.995185311	5.937%
N-acetyl-2-phenylethylamine	C10 H13 N O	NA	Carboxylic acids and	-3.25	163.09971	163.09918	7.366	14791860.87	0.010242539	0.015%

			derivatives							
4-[(Butylcarbamoyl)amino]-1-ethyl-1H-pyrazole-5-carboxamide	C11 H19 N5 O2	NA	Carboxylic acids and derivatives	-3.45	253.15387	253.153	1.386	352189019.1	0.243871257	0.362%
3-(1-hydroxyethyl)-2,3,6,7,8,8a-hexahydropyrrolo[1,2-a]pyrazine-1,4-dione	C9 H14 N2 O3	NA	Carboxylic acids and derivatives	-2.58	198.10044	198.09993	1.739	570378681.1	0.394955432	0.587%
NCGC00169940-02!3-(1H-indol-3-ylmethyl)-2,3,6,7,8,8a-hexahydropyrrolo[1,2-a]pyrazine-1,4-dione	C16 H17 N3 O2	NA	Carboxylic acids and derivatives	-4.02	283.13208	283.13094	7.064	16533822.9	0.01144875	0.017%
N-Fructosyl phenylalanine	C15 H21 N O7	NA	Carboxylic acids and derivatives	-2.86	327.1318	327.13087	1.923	247535878.6	0.171404793	0.255%
N-Fructosyl isoleucine	C12 H23 N O7	NA	Carboxylic acids and derivatives	-3.43	293.14745	293.14645	1.275	459451270.2	0.318144385	0.473%
Isoleucylglutamate	C11 H20 N2 O5	NA	Carboxylic acids and derivatives	-3.28	260.13722	260.13637	1.333	132951162.2	0.092061266	0.137%
3-hydroxy-C6-homoserine lactone	C10 H17 N O4	NA	Carboxylic acids and derivatives	-2.92	215.11576	215.11513	3.875	48833518.02	0.033814488	0.050%
NCGC00380813-01!methyl 2-(2-hydroxypropanoylamino)-3-methylbutanoate	C9 H17 N O4	NA	Carboxylic acids and derivatives	-3.31	203.11576	203.11509	1.528	59815742.02	0.041419066	0.062%
D-(-)-Aspartic acid	C4 H7 N O4	1783-96-6	Carboxylic acids and derivatives	-2.34	133.03751	133.0372	0.869	136881012.2	0.094782468	0.141%
NCGC00381347-01!5-acetamido-4-oxohexanoic acid	C8 H13 N O4	NA	Keto acids and derivatives	-2.98	187.08446	187.0839	1.344	184139348.6	0.127506231	0.189%
5-Nitro-2-(1,2,3,6-tetrahydropyridin-1-yl)pyridine	C10 H11 N3 O2	NA	Allyl-type 1,3-dipolar organic compounds	-2.81	205.08513	205.08455	2.825	83241060.08	0.057639793	0.086%
Phloretin	C15 H14 O5	60-82-2	Linear 1,3-diarylpropanoids	-4.9	274.08412	274.08278	8.329	7217225.504	0.004997526	0.007%
Aflatoxin G2	C17 H14 O7	7241-98-7	Coumarins and derivatives	-4.78	330.07395	330.07237	9.739	79991308.54	0.055389521	0.082%
Coumarin	C9 H6 O2	91-64-5	Coumarins and derivatives	-4.31	146.03678	146.03615	9.919	71479875.69	0.049495828	0.074%
Senkyunolide A	C12 H16 O2	63038-10-8	Isobenzofurans	-4.07	192.11503	192.11425	11	12460045.44	0.008627887	0.013%
2-(2,5-Dimethyl-1H-pyrrol-1-yl)isoindoline-1,3-dione	C14 H12 N2 O2	NA	Isoindoles and derivatives	-3.63	240.08988	240.08901	6.089	24641778	0.017063057	0.025%
4-Indolecarbaldehyde	C9 H7 N O	1074-86-6	Indoles and derivatives	-3.08	145.05276	145.05232	4.255	50350222.91	0.034864722	0.052%
trans-3-Indoleacrylic acid	C11 H9 N O2	1204-06-4	Indoles and derivatives	-3.62	187.06333	187.06265	4.279	373507291.3	0.258632972	0.384%
Indole	C8 H7 N	120-72-9	Indoles and derivatives	-1.5	117.05785	117.05767	4.257	417271855.1	0.288937492	0.429%
Norharman	C11 H8 N2	244-63-3	Indoles and derivatives	-3.21	168.06875	168.06821	5.752	98454678.15	0.068174375	0.101%
2,3,4,9-Tetrahydro-1H-β-carboline-3-carboxylic acid	C12 H12 N2 O2	42438-90-4	Indoles and derivatives	-3.26	216.08988	216.08917	5.304	90482329.61	0.062653968	0.093%
Indoline	C8 H9 N	496-15-1	Indoles and derivatives	-1.57	119.0735	119.07331	2.759	157517116.6	0.10907182	0.162%
3-(2-Hydroxyethyl)indole	C10 H11 N O	526-55-6	Indoles and derivatives	-4.27	161.08406	161.08338	9.82	17346717.97	0.012011635	0.018%
5-Hydroxyindole-3-acetic acid	C10 H9 N O3	54-16-0	Indoles and derivatives	-3.36	191.05824	191.0576	6.172	18127456.79	0.012552253	0.019%
NCGC00380254-01_C17H21N3O3_10b-Hydroxy-3-isobutyl-6,10b,11,11a-tetrahydro-2H-pyrazino[1',2':1,5]pyrrolo[2,3-b]indole-1,4(3H,5aH)-dione	C17 H21 N3 O3	NA	Indoles and derivatives	-4	315.15829	315.15703	7.706	8697180.77	0.006022313	0.009%
4-(Dimethylamino)pyridine	C7 H10 N2	1122-58-3	Organonitrogen compounds	-2.29	122.0844	122.08412	1.107	55736347.47	0.038594313	0.057%
2-Aminooctadec-4-yne-1,3-diol	C18 H35 N O2	20256-56-8	Organonitrogen compounds	-3.67	297.26678	297.26569	11.051	47271344.6	0.03273277	0.049%
Dehydrophytosphingosine (not validated, isomer of 1679)	C18 H37 N O3	3687-54-5	Organonitrogen compounds	-4.3	315.27734	315.27599	10.762	45718295.22	0.03165737	0.047%
L(-)-Carnitine	C7 H15 N O3	541-15-1	Organonitrogen compounds	-3.49	161.10519	161.10463	0.802	734144217.2	0.508353934	0.755%
2-Amino-1,3,4-octadecanetriol	C18 H39 N O3	554-62-1	Organonitrogen compounds	-4.07	317.29299	317.2917	11.153	44821062.95	0.031036087	0.046%
α-Linolenoyl ethanolamide	C20 H35 N O2	57086-93-8	Organonitrogen compounds	-4.58	321.26678	321.26531	15.411	6418055.106	0.004444145	0.007%
Choline	C5 H13 N O	62-49-7	Organonitrogen compounds	0.41	103.09971	103.09976	0.762	4651086937	3.220618356	4.786%
Gaboxadol	C6 H8 N2 O2	64603-91-4	Organonitrogen compounds	-2.11	140.05858	140.05828	1.109	1146552525	0.793923691	1.180%
Linoleoyl Ethanolamide	C20 H37 N O2	68171-52-8	Organonitrogen compounds	-4.07	323.28243	323.28111	14.322	6677165.632	0.004623565	0.007%
Triethyl phosphate	C6 H15 O4 P	78-40-0	Organic phosphoric acids and derivatives	-3.48	182.0708	182.07016	7.679	7055314.543	0.004885412	0.007%
Glutamylphenylalanine (isomer of 1503)	C14 H18 N2 O5	NA	Organic carbonic acids and derivatives	-3.54	294.12157	294.12053	5.049	28075774.76	0.019440908	0.029%

4-Hydroxybenzaldehyde	C7 H6 O2	123-08-0	Organooxygen compounds	-1.97	122.03678	122.03654	5.959	31311738.38	0.021681633	0.032%
Cathinone	C9 H11 N O	16735-19-6	Organooxygen compounds	-3.49	149.08406	149.08354	9.224	8612663.729	0.005963789	0.009%
MALTOSE	C12 H22 O11	16984-36-4	Organooxygen compounds	-3.57	342.11621	342.11499	0.882	108770175.1	0.075317281	0.112%
Muscone	C16 H30 O	541-91-3	Organooxygen compounds	-4.05	238.22967	238.2287	16.957	18171146.06	0.012582505	0.019%
5-Hydroxymethyl-2-furaldehyde	C6 H6 O3	67-47-0	Organooxygen compounds	-2.35	126.03169	126.0314	0.893	509396912.8	0.352728958	0.524%
Isophorone	C9 H14 O	78-59-1	Organooxygen compounds	-3.18	138.10447	138.10403	8.577	20233742.71	0.014010739	0.021%
Pantothenic acid	C9 H17 N O5	79-83-4	Organooxygen compounds	-3.22	219.11067	219.10997	2.523	240252318.1	0.166361334	0.247%
Acetophenone	C8 H8 O	98-86-2	Organooxygen compounds	-1.76	120.05751	120.0573	1.25	82184852.91	0.056908428	0.085%
3-Aminoacetophenon	C8 H9 N O	99-03-6	Organooxygen compounds	-2.12	135.06841	135.06813	1.18	204950323.9	0.141916671	0.211%
NCGC00380144-01_C20H28O3_(8E)-14-Hydroxy-5,9,12,13-tetramethyl-16-methylene-4-oxatricyclo[10.3.1.0~3,5~]hexadeca-1(15),8-dien-2-one	C20 H28 O3	NA	Organooxygen compounds	-4.66	316.20384	316.20237	9.1	6683333.605	0.004627836	0.007%
[1,2,3]Triazolo[4,5-f]benzotriazole-4,8(1H,5H)-dione	C6 H2 N6 O2	NA	Organooxygen compounds	-0.94	190.02392	190.02374	0.763	391695534.9	0.271227317	0.403%
5-aminoimidazole ribotide	C8 H14 N3 O7 P	25635-88-5	Organooxygen compounds	2.37	295.05694	295.05763	0.725	876014248	0.60659102	0.901%
(2R,3R,4R)-4-Hydroxy-2-(hydroxymethyl)-3-pyrrolidinyl 4-O-(6-deoxy-beta-D-glucopyranosyl)-alpha-D-glucopyranoside	C17 H31 N O12	736967-62-7	Organooxygen compounds	-2.92	441.18463	441.18334	1.309	455685420.1	0.315536744	0.469%
Perillartine	C10 H15 N O	30950-27-7	Prenol lipids	-2.99	165.11536	165.11487	5.112	42431334.08	0.029381333	0.044%
NCGC00384758-01_C27H40O5_(2alpha,3beta,5alpha,8xi,14xi,25S)-2,3-Dihydroxyspirost-9(11)-en-12-one	C27 H40 O5	3514-48-5	Prenol lipids	-3.89	444.28757	444.28584	8.118	6174663.146	0.00427561	0.006%
Nootkatone	C15 H22 O	4674-50-4	Prenol lipids	-2.98	218.16707	218.16642	6.811	32156514.49	0.022266593	0.033%
Isoalantolactone	C15 H20 O2	470-17-7	Prenol lipids	-4.78	232.14633	232.14522	8.151	17157329.82	0.011880494	0.018%
Diosgenin	C27 H42 O3	512-04-9	Prenol lipids	-4.33	414.3134	414.3116	9.91	4639654.922	0.003212702	0.005%
Quillaic acid	C30 H46 O5	631-01-6	Prenol lipids	-3.9	486.33452	486.33263	7.56	5316408.881	0.003681317	0.005%
Carvone	C10 H14 O	6485-40-1	Prenol lipids	-3.57	150.10447	150.10393	10.593	10582940.18	0.007328096	0.011%
(3aS,10aR,10bR)-6,10a-Dimethyl-3-methylene-3,3a,4,5,7,8,10a,10b-octahydrofuro[3',2':6,7]cyclohepta[1,2-b]pyran-2,9-dione	C15 H18 O4	6995-02-4	Prenol lipids	-3.76	262.12051	262.11952	7.058	32193737.13	0.022292368	0.033%
Plumericin	C15 H14 O6	77-16-7	Prenol lipids	-4.46	290.07904	290.07775	7.619	4726989.801	0.003273177	0.005%
NCGC00169469-03_C20H34O3_1-Naphthalenecarboxylic acid, decahydro-5-(5-hydroxy-3-methylpentyl)-1,4a-dimethyl-6-methylene-, (1R,4aS,5R,8aS)-	C20 H34 O3	NA	Prenol lipids	-4.63	322.25079	322.2493	10.023	41070701.95	0.028439171	0.042%
(3aR,4aS,5R,7aS,8S,9aR)-5-Hydroxy-4a,8-dimethyl-3-methyleneoctahydroazuleno[6,5-b]furan-2,6(3H,4H)-dione	C15 H20 O4	NA	Prenol lipids	-4.06	264.13616	264.13509	7.597	19322607.17	0.013379828	0.020%
(1S,4aS,5R)-5-[2-(3-Furyl)ethyl]-1,4a-dimethyl-6-methylenedecahydro-1-naphthalenecarboxylic acid	C20 H28 O3	NA	Prenol lipids	-3.81	316.20384	316.20264	7.358	19305471.1	0.013367962	0.020%
(1R,4aS,5R,8aS)-5-(5-hydroxy-3-methylpentyl)-1,4a-dimethyl-6-methylidene-3,4,5,7,8,8a-hexahydro-2H-naphthalene-1-carboxylic acid	C20 H34 O3	NA	Prenol lipids	-4.59	322.25079	322.24932	8.983	10789936.99	0.00747143	0.011%
D-(+)-Camphor	C10 H16 O	464-49-3	Prenol lipids	-4.03	152.12012	152.1195	8.807	38300563.01	0.026521004	0.039%
phenylethylamide 359	C24 H41 N O	10015-69-7	Fatty Acyls	-3.77	359.31881	359.31746	19.274	5589126.857	0.003870159	0.006%
cis,cis-Muconic acid	C6 H6 O4	1119-72-8	Fatty Acyls	-2.1	142.02661	142.02631	2.227	193864225.5	0.134240166	0.199%
Azelaic acid	C9 H16 O4	123-99-9	Fatty Acyls	-2.96	188.10486	188.1043	3.464	41371802.81	0.028647667	0.043%
Dethiobiotin	C10 H18 N2 O3	533-48-2	Fatty Acyls	-2.75	214.13174	214.13115	1.363	68055501.22	0.04712464	0.070%

9-Oxo-10(E),12(E)-octadecadienoic acid	C18 H30 O3	54232-59-6	Fatty Acyls	-3.93	294.21949	294.21834	13.557	20230886.93	0.014008761	0.021%
Jasmonic acid	C12 H18 O3	59366-47-1	Fatty Acyls	-3.91	210.12559	210.12477	11.001	15804467.48	0.010943712	0.016%
5-Aminovaleric acid betaine	C8 H17 N O2	6778-33-2	Fatty Acyls	-2.85	159.12593	159.12547	1.098	340706504.7	0.235920256	0.351%
9-methoxycarbonyldec-9-enoic acid	C12 H20 O4	913690-67-2	Fatty Acyls	-3.96	228.13616	228.13526	10.997	12683950.18	0.008782928	0.013%
(9Z,12E)-15,16-dihydroxyoctadeca-9,12-dienoic acid	C18 H32 O4	NA	Fatty Acyls	-4.21	312.23006	312.22875	10.688	42638287.33	0.029524636	0.044%
8-{3-Oxo-2-[(2E)-2-penten-1-yl]-1-cyclopenten-1-yl}octanoic acid	C18 H28 O3	NA	Fatty Acyls	-4.62	292.20384	292.20249	12.91	19019165.06	0.013169711	0.020%
13(S)-HOTrE	C18 H30 O3	NA	Fatty Acyls	-4.07	294.21949	294.2183	10.706	37767948.28	0.026152198	0.039%
Ceratodictyol	C19 H38 O4	NA	Fatty Acyls	-4.19	330.27701	330.27562	16.958	192977903.7	0.133626438	0.199%
α-Eleostearic acid	C18 H30 O2	NA	Fatty Acyls	-4.18	278.22458	278.22342	11.91	46565078.42	0.03224372	0.048%
Methanandamide	C23 H39 N O2	NA	Fatty Acyls	-3.96	361.29808	361.29665	17.917	8383562.244	0.005805149	0.009%
Dehydro-piliformic-acid	C11 H16 O4	NA	Fatty Acyls	-3.52	212.10486	212.10411	6.14	39234390.53	0.027167628	0.040%
6-Aminocaproic acid	C6 H13 N O2	60-32-2	Fatty Acyls	-2.61	131.09463	131.09429	0.837	202650643.2	0.14032427	0.209%
Phenazone	C11 H12 N2 O	60-80-0	Azoles	-4.09	188.09496	188.09419	8.484	5570316.785	0.003857134	0.006%
Desthiobiotin	C10 H18 N2 O3	15720-25-9	Azoles	-3.14	214.13174	214.13107	2.986	39955287.29	0.027666809	0.041%
Ethyl 5-(tert-butyl)-1H-pyrazole-3-carboxylate	C10 H16 N2 O2	294852-57-6	Azoles	-3.42	196.12118	196.12051	1.104	839992964.3	0.581648289	0.864%
5-[(4-Chlorobenzoyl)amino]-2-{4-[(2,6-dichlorobenzyl)oxy]phenyl}-1,3-oxazole-4-carboxylic acid	C24 H15 Cl3 N2 O5	NA	Azoles	-2.66	516.00465	516.00328	0.763	367293528.1	0.254330288	0.378%
Rilmenidine	C10 H16 N2 O	54187-04-1	Azolines	-3.36	180.12626	180.12566	1.526	76034973.51	0.052649979	0.078%

Description of table parameters

Name	Compound name
Formula	Chemical formula
CAS_num	CAS number of the compound
Class	Compound classification information
Annot. DeltaMass [ppm]	Detection bias of annotated compounds
Annotation MW	Annotate the Molecular Weight value of the compound theory
Calc. MW	Molecular Weight value of the assay
RT [min]	Retention time
Area	Detected peak area

Negative Mode

Name	Formula	CAS_num	Class	Annot. DeltaMass [ppm]	Annotation MW	Calc. MW	RT [min]	Area	Relative concentrations of components in Huaier (μg/ml)	Relative percentage of constituents in Huaier (%)
2-[5-({(3E)-3-[(5-Nitro-2-pyridinyl)imino]butanoyl}amino)-1,3,4-thiadiazol-2-yl]phenyl acetate	C19 H16 N6 O5 S	NA	Phenol esters	2.9	440.09029	440.09157	1.166	2098970369	15.52912813	3.729%
Octyl gallate	C15 H22 O5	1034-01-1	Benzene and substituted derivatives	-1.64	282.14672	282.14626	5.869	70689089.94	0.522989725	0.126%
2,2'-Methylenebis(4-methyl-6-tert-butylphenol)	C23 H32 O2	119-47-1	Benzene and substituted derivatives	-2.37	340.24023	340.23942	16.709	274416669.3	2.030258113	0.488%
Monobenzyl phthalate	C15 H12 O4	2528-16-7	Benzene and substituted derivatives	-1.84	256.07356	256.07309	9.451	10482805.3	0.077556515	0.019%
2-{[(4-Chlorophenyl)carbamoyl]amino}-6-ethyl-4,5,6,7-tetrahydrothieno[2,3-c]pyridine-3-carboxamide	C17 H19 Cl N4 O2 S	NA	Benzene and substituted derivatives	1.6	378.09172	378.09233	0.786	8257715857	61.09430107	14.670%
4,6,8-trihydroxy-7-methoxy-3-methyl-3,4-dihydroisochromen-1-one	C11 H12 O6	NA	Benzene and substituted derivatives	-2.82	240.06339	240.06271	5.556	63746376.93	0.471624407	0.113%
N-[(2S)-2-(3,4-Dichlorophenyl)-4-(1-oxido-1'H-spiro[1-benzothiophene-3,4'-piperidin]-1'-yl)butyl]-N-methyl-4-biphenylsulfonamide	C35 H36 Cl2 N2 O3 S2	NA	Benzene and substituted derivatives	-4.41	666.15444	666.1515	0.835	285909859.3	2.115289909	0.508%
5-carboxyvanillic acid	C9 H8 O6	2134-91-0	Benzene and substituted derivatives	-4.32	212.03209	212.03117	5.658	433882736.9	3.210059903	0.771%
lissoclibadin 2	C26 H38 N2 O4 S5	NA	Benzene and substituted derivatives	2.83	602.14351	602.14522	0.789	301325201.9	2.229339556	0.535%
4-Pyridoxate	C8 H9 N O4	82-82-6	Pyridines and derivatives	-4.91	183.05316	183.05226	1.432	51389929.96	0.380205847	0.091%
Methyl 1-ethoxy-4-hydroxy-5-oxo-2,5-dihydro-1H-pyrrole-3-carboxylate	C8 H11 N O5	NA	Pyrrolines	-4.63	201.06372	201.06279	1.301	594241945.7	4.396469553	1.056%
1-(2-Furylmethyl)-5-oxopyrrolidine-3-carboxylic acid	C10 H11 N O4	175136-93-3	Pyrrolidines	-3.9	209.06881	209.06799	5.613	22820032.79	0.16883288	0.041%
Benzoic acid + 1O, 1MeO, O-Hex	C14 H18 O9	NA	Tannins	-0.94	330.09508	330.09477	2.79	14980177.02	0.110830096	0.027%
Riboflavin	C17 H20 N4 O6	83-88-5	Pteridines and derivatives	-1.53	376.13828	376.13771	5.701	31362662.66	0.232035104	0.056%
N-(4-Bromophenyl)-4-[4-methyl-3-(4-morpholinylsulfonyl)phenyl]-1-phthalazinamine	C25 H23 Br N4 O3 S	NA	Diazines	3.23	538.06742	538.06916	0.903	600278844	4.441133245	1.066%
N-(3,4,5-Trifluorobenzyl)-6-(trifluoromethyl)-2-{4-[3-(trifluoromethyl)-2-pyridinyl]-1-piperazinyl}-1H-benzimidazol-4-amine	C25 H19 F9 N6	NA	Diazinanes	-4.4	574.15275	574.15022	0.801	405103553.7	2.997138543	0.720%
5,7-Dihydroxy-2-(4-hydroxyphenyl)-6-[3,4,5-trihydroxy-6-(hydroxymethyl)oxan-2-yl]-8-(3,4,5-trihydroxyoxan-2-yl)chromen-4-one	C26 H28 O14	207461-10-7	Flavonoids	-1.3	564.14791	564.14717	6.229	29104444.19	0.215327786	0.052%
5,7-Dihydroxy-2-(4-hydroxyphenyl)-6,8-bis[3,4,5-trihydroxy-6-(hydroxymethyl)tetrahydro-2H-pyran-2-yl]-4H-chromen-4-one	C27 H30 O15	23666-13-9	Flavonoids	-1.45	594.15847	594.15761	5.635	10046625.73	0.074329462	0.018%
(-)-Epicatechin	C15 H14 O6	490-46-0	Flavonoids	-1.21	290.07904	290.07869	7.637	10651408.37	0.078803916	0.019%
Isoschaftoside	C26 H28 O14	52012-29-0	Flavonoids	-1.23	564.14791	564.14721	5.841	47340414.3	0.350245706	0.084%
Tricin	C17 H14 O7	520-32-1	Flavonoids	-1.65	330.07395	330.07341	9.749	110610451.1	0.818345934	0.197%
5,9-Dihydroxy-2-(2-hydroxy-2-propanyl)-1-(1-hydroxy-3,5,6-trimethoxy-10-methyl-9-oxo-9,10-dihydro-2-acridinyl)-10-methoxy-11-methyl-1,11-dihydrofuro[2,3-c]acridin-6(2H)-one	C37 H36 N2 O11	NA	Quinolines and derivatives	-0.13	684.23191	684.23182	0.794	449599836.8	3.326342086	0.799%
4-(4-Fluorobenzyl)-3-[(4-methylbenzyl)sulfanyl]-5-(trifluoromethyl)-4H-1,2,4-triazole	C18 H15 F4 N3 S	NA	Thioethers	0.69	381.09228	381.09254	0.786	337080794.5	2.493875534	0.599%
1-Deoxy-1-{2,6,8-trioxo-7-[3-(phosphonooxy)propyl]-1,2,3,6,7,8-hexahydro-9H-purin-9-yl}-D-ribitol	C13 H21 N4 O11 P	NA	Imidazopyrimidines	-4.67	440.09444	440.09239	0.796	2326836529 7	172.1498462	41.337%
Uridine monophosphate (UMP)	C9 H13 N2 O9 P	58-97-9	Pyrimidine nucleotides	-1.77	324.03587	324.03529	0.826	74056935.73	0.547906565	0.132%
Cefsumide	C17 H20 N4 O6 S2	54818-11-0	Lactams	3.57	440.08243	440.084	1.186	1786836977	13.21982472	3.174%

Guanosine	C10 H13 N5 O5	118-00-3	Purine nucleosides	-1.65	283.09167	283.0912	1.266	78813876.68	0.583100556	0.140%
Guanosine monophosphate (GMP)	C10 H14 N5 O8 P	85-32-5	Purine nucleotides	-1.34	363.058	363.05751	1.101	78404260.83	0.580070034	0.139%
Piceatannol	C14 H12 O4	10083-24-6	Stilbenes	-2.55	244.07356	244.07294	9.147	11752030.57	0.086946815	0.021%
3-O-Undecyl-D-glucopyranose	C17 H34 O6	NA	Others	-0.43	334.23554	334.2354	17.286	1024294742	7.578193832	1.820%
NCGC00380353-01_C15H18O6_Pentaleno[1,6a-c]pyran-9-carboxylic acid, 1,3,4,7,7a,9a-hexahydro-4-hydroxy-4-(hydroxymethyl)-6,7-dimethyl-3-oxo-, (4R,7S,7aR,9aR)-	C15 H18 O6	NA	Others	-1.36	294.11034	294.10994	4.014	104966034.4	0.776585998	0.186%
NCGC00384563-01!5,7-dihydroxy-2-(4-hydroxyphenyl)-6,8-bis(3,4,5-trihydroxyoxan-2-yl)chromen-4-one	C25 H26 O13	NA	Others	-1.02	534.13734	534.13679	6.368	33348834.63	0.246729698	0.059%
(E)-3,4,5-Trimethoxycinnamic acid	C12 H14 O5	20329-98-0	Others	-2.9	238.08412	238.08343	6.295	2049223748	15.16108023	3.641%
3-Amino-N-(4-methylbenzyl)-4-(trifluoromethyl)-6,7-dihydro-5H-cyclopenta[b]thieno[3,2-e]pyridine-2-carboxamide	C20 H18 F3 N3 O S	NA	Others	-2.59	405.11227	405.11122	0.794	296405366.2	2.192940396	0.527%
10-Hydroxydecanoic acid	C10 H20 O3	1679-53-4	Hydroxy acids and derivatives	-3.78	188.14124	188.14053	8.81	77491618.77	0.573317897	0.138%
Hydroxysebacic acid	C10 H18 O5	73141-46-5	Hydroxy acids and derivatives	-3.53	218.11542	218.11465	6.789	107400588.2	0.794597923	0.191%
2-(6-Hydroxyhexyl)-3-methylenesuccinic acid	C11 H18 O5	NA	Hydroxy acids and derivatives	-2.95	230.11542	230.11474	6.676	30979752.41	0.229202161	0.055%
Diferuloyl putrescine	C24 H28 N2 O6	42369-86-8	Cinnamic acids and derivatives	-1.02	440.19474	440.19429	8.261	13714557.27	0.101466472	0.024%
Ferulic acid	C10 H10 O4	537-98-4	Cinnamic acids and derivatives	-4.81	194.05791	194.05697	6.848	29067870.89	0.215057201	0.052%
Dicoumaroyl Spermidine	C25 H31 N3 O4	65715-79-9	Cinnamic acids and derivatives	-1.74	437.23146	437.2307	6.358	23015455.92	0.170278709	0.041%
ATPA	C10 H16 N2 O4	140158-50-5	Carboxylic acids and derivatives	-3.19	228.11101	228.11028	4.772	250309747.4	1.851904248	0.445%
(2S,4S)-4-hydroxy-2,3,4,5-tetrahydrodipicolinic acid	C7 H9 N O5	185103-33-7	Carboxylic acids and derivatives	-4.99	187.04807	187.04714	1.132	270196755.6	1.999037291	0.480%
2-Aminooctanedioic acid	C8 H15 N O4	19641-59-9	Carboxylic acids and derivatives	-4.93	189.10011	189.09918	1.398	131563706.4	0.973367554	0.234%
N-Acetyl-L-phenylalanine	C11 H13 N O3	2018-61-3	Carboxylic acids and derivatives	-4.53	207.08954	207.08861	6.687	18681878.67	0.138216952	0.033%
3-Hydroxy-3-(methoxycarbonyl)pentanedioic acid	C7 H10 O7	26163-65-5	Carboxylic acids and derivatives	-4.32	206.04265	206.04176	1.676	178006621.1	1.316973155	0.316%
Ala-Phe	C12 H16 N2 O3	3061-90-3	Carboxylic acids and derivatives	-2.35	236.11609	236.11554	4.286	15202312	0.112473551	0.027%
Ala-Leu	C9 H18 N2 O3	3303-34-2	Carboxylic acids and derivatives	-4.23	202.13174	202.13089	2.715	45160386.44	0.334116879	0.080%
Kainic acid	C10 H15 N O4	487-79-6	Carboxylic acids and derivatives	-3.78	213.10011	213.0993	7.807	18174322.88	0.134461826	0.032%
Leucylproline	C11 H20 N2 O3	6403-35-6	Carboxylic acids and derivatives	-3.19	228.14739	228.14667	3.573	30327795.94	0.224378694	0.054%
ulixertinib	C21 H22 Cl2 N4 O2	869886-67-9	Carboxylic acids and derivatives	-2.35	432.11198	432.11097	1.038	350896892.8	2.596093252	0.623%
(-)-Spiculisporic acid	C17 H28 O6	NA	Carboxylic acids and derivatives	-1.88	328.18859	328.18797	12.074	7453281.415	0.055142733	0.013%
NCGC00384508-01!2-[2-[(5R,6R,7S,9S,11R,18S,19S)-19-amino-6-(3,4-dicarboxybutanoyloxy)-11,16,18-trihydroxy-5,9-dimethylicosan-7-yl]oxy-2-oxoethyl]butanedioic acid	C34 H59 N O15	NA	Carboxylic acids and derivatives	-0.21	721.38847	721.38832	8.922	11220046.65	0.083010958	0.020%
N-Fructosyl pyroglutamate	C11 H17 N O8	NA	Carboxylic acids and	-1.19	291.09542	291.09507	1.103	54964622.09	0.406653029	0.098%

			derivatives							
Isoleucylisoleucine	C12 H24 N2 O3	NA	Carboxylic acids and derivatives	-2.53	244.17869	244.17807	5.359	49398746.5	0.365474175	0.088%
(2R,3S)-N-[(3S)-1-(3-Anilinobenzyl)-2-oxo-3-azepanyl]-2-isobutyl-3-propylsuccinamide	C30 H42 N4 O3	NA	Carboxylic acids and derivatives	-4.09	506.32569	506.32362	10.535	457463568.7	3.384521516	0.813%
4-[(4-{(E)-[3-(2-Ethoxy-2-oxoethyl)-2,4-dioxo-1,3-thiazolidin-5-ylidene]methyl}phenoxy)methyl]benzoic acid	C22 H19 N O7 S	NA	Carboxylic acids and derivatives	-4.04	441.08822	441.08644	0.989	250977656.6	1.85684574	0.446%
N-(6-Amino-1-butyl-2,4-dioxo-1,2,3,4-tetrahydro-5-pyrimidinyl)-N-isobutyl-2-(7,7,9-trimethyl-2,4-dioxo-1,3-diazaspiro[4.5]dec-3-yl)acetamide	C25 H40 N6 O5	NA	Carboxylic acids and derivatives	4.41	504.30602	504.30824	10.543	414682753.9	3.068009781	0.737%
N-[(2Z)-2-(Benzoylamino)-3-(4-fluorophenyl)-2-propenoyl]tryptophan	C27 H22 F N3 O4	NA	Carboxylic acids and derivatives	-2.58	471.15943	471.15822	1.138	981290768.3	7.260031063	1.743%
Bestatin	C16 H24 N2 O4	58970-76-6	Peptidomimetics	-1.71	308.17361	308.17308	10.538	9080889.661	0.067184512	0.016%
Murrangatin	C15 H16 O5	37126-91-3	Coumarins and derivatives	-0.77	276.09977	276.09956	6.658	11832412.6	0.087541518	0.021%
DL-Tryptophan	C11 H12 N2 O2	54-12-6	Indoles and derivatives	-4.44	204.08988	204.08897	4.37	45746975.12	0.338456726	0.081%
5-Hydroxyindole-3-acetic acid	C10 H9 N O3	54-16-0	Indoles and derivatives	-3.53	191.05824	191.05757	6.205	65205404.35	0.482418949	0.116%
Porphobilinogen	C10 H14 N2 O4	487-90-1	Organonitrogen compounds	-3.24	226.09536	226.09463	2.486	249244123.3	1.84402028	0.443%
Pantothenic acid	C9 H17 N O5	79-83-4	Organooxygen compounds	-3.63	219.11067	219.10988	2.645	216434228.8	1.601277904	0.385%
1,4-D-xylobiose	C10 H18 O9	NA	Organooxygen compounds	-1.14	282.09508	282.09476	0.822	488725217.2	3.615809272	0.868%
Trehalose-6-Phosphate	C12 H23 O14 P	4484-88-2	Organooxygen compounds	-0.82	422.08254	422.0822	0.711	79593464.45	0.588868298	0.141%
Glucose 1-phosphate	C6 H13 O9 P	59-56-3	Organooxygen compounds	-1.8	260.02972	260.02925	0.716	94394757.81	0.698374932	0.168%
α,α-Trehalose	C12 H22 O11	99-20-7	Organooxygen compounds	-1.99	342.11621	342.11553	0.787	3830184809	28.33743228	6.804%
deaminoneuraminic acid	C9 H16 O9	153666-19-4	Organooxygen compounds	-1.87	268.07943	268.07893	0.836	1228218111	9.086910758	2.182%
Azuleno(5,6-c)furan-1(3H)-one, 4,4a,5,6,7,7a,8,9-octahydro-3,4,8-trihydroxy-6,6,8-trimethyl-	C15 H22 O5	71305-94-7	Prenol lipids	-1.45	282.14672	282.14631	5.339	9839066.584	0.072793846	0.017%
Dihydroartemisinin	C15 H24 O5	71939-50-9	Prenol lipids	-1.74	284.16237	284.16188	7.614	7855780.77	0.058120604	0.014%
(3aR,4R,6E,10Z,11aR)-4-hydroxy-10-(hydroxymethyl)-3-methylidene-2-oxo-3a,4,5,8,9,11a-hexahydrocyclodeca[b]furan-6-carbaldehyde	C15 H18 O5	NA	Prenol lipids	-2.17	278.11542	278.11482	6.117	61734487.47	0.456739543	0.110%
(E)-2-(hydroxymethyl)-3-(3-oxo-5-propan-2-yl-4,5,6,7-tetrahydro-1H-2-benzofuran-4-yl)prop-2-enoic acid	C15 H20 O5	NA	Prenol lipids	-1.81	280.13107	280.13057	6.241	50448791.61	0.373242882	0.090%
8-hydroxy-5,8a-dimethyl-3-methylidene-3a,4,4a,8,9,9a-hexahydrobenzo[f][1]benzofuran-2,7-dione	C15 H18 O4	NA	Prenol lipids	-1.91	262.12051	262.12001	7.528	20167472.47	0.149208045	0.036%
3-tert-Butyladipic acid	C10 H18 O4	10347-88-3	Fatty Acyls	-4.54	202.12051	202.11959	8.586	365954390	2.707495398	0.650%
Dibutyl Fumarate	C12 H20 O4	105-75-9	Fatty Acyls	-3.26	228.13616	228.13541	10.99	285978185.6	2.115795417	0.508%
Oleic acid alkyne	C18 H30 O2	151333-45-8	Fatty Acyls	-2.26	278.22458	278.22395	15.784	8037363.991	0.059464039	0.014%
8-Iso-15-keto-prostaglandin-F2β	C20 H32 O5	191919-01-4	Fatty Acyls	-1.38	352.22497	352.22449	7.347	51964939.82	0.384460029	0.092%
beta-Hydroxymyristic acid	C14 H28 O3	1961-72-4	Fatty Acyls	-2.58	244.20384	244.20321	13.235	4019796.675	0.029740266	0.007%
(+/-)12(13)-DiHOME	C18 H34 O4	263399-35-5	Fatty Acyls	-1.16	314.24571	314.24534	10.837	11506688.1	0.085131661	0.020%
palmitic acid	C16 H32 O2	57-10-3	Fatty Acyls	-2.37	256.24023	256.23962	18.106	54956984.49	0.406596523	0.098%
Linoleic acid	C18 H32 O2	60-33-3	Fatty Acyls	-2.66	280.24023	280.23948	17.084	82019046.9	0.606813849	0.146%
FA 18:1+1O	C18 H34 O3	61789-44-4	Fatty Acyls	-1.8	298.25079	298.25026	13.495	16411109.1	0.121416776	0.029%
(+/-)9-HpODE	C18 H32 O4	67597-24-4	Fatty Acyls	-1.48	312.23006	312.2296	12.468	9165810.916	0.067812797	0.016%
Dodecanedioic acid	C12 H22 O4	693-23-2	Fatty Acyls	-2.92	230.15181	230.15114	6.177	18147937.38	0.134266614	0.032%
(+/-)9-HODE	C18 H32 O3	98524-19-7	Fatty Acyls	-2.14	296.23514	296.23451	12.863	7440170.975	0.055045736	0.013%
(15Z)-9,12,13-Trihydroxy-15-octadecenoic acid	C18 H34 O5	NA	Fatty Acyls	-1.62	330.24062	330.24009	9.854	1215660188	8.994001588	2.160%
1-(3,5-Dihydroxyphenyl)-12-hydroxy-2-tridecanyl acetate	C21 H34 O5	NA	Fatty Acyls	-2.11	366.24062	366.23985	9.701	5134531.418	0.037987576	0.009%
9-(2,3-dihydroxypropoxy)-9-oxononanoic acid	C12 H22 O6	NA	Fatty Acyls	-1.72	262.14164	262.14119	7.013	35645858.82	0.263724118	0.063%
FA 18:3+2O	C18 H30 O4	NA	Fatty Acyls	-1.41	310.21441	310.21397	12.563	15422107.9	0.1140997	0.027%
(+/-)9,10-dihydroxy-12Z-octadecenoic acid	C18 H34 O4	NA	Fatty Acyls	-1.55	314.24571	314.24522	11.916	147476523	1.091097739	0.262%
13(S)-HOTrE	C18 H30 O3	NA	Fatty Acyls	-1.32	294.21949	294.21911	13.397	18427342.56	0.13633378	0.033%
13-HpOTrE	C18 H30 O4	NA	Fatty Acyls	-1.61	310.21441	310.21391	11.801	16686528.94	0.123454457	0.030%
RKI-1447	C16 H14 N4 O2 S	1342278-01-6	Azoles	1.66	326.08375	326.08429	0.833	314380594.4	2.32592923	0.559%

Supplementary Table 1 Components of Huaier identified by HPLC-MS/MS

Description of table parameters	
Name	Compound name
Formula	Chemical formula
CAS_num	CAS number of the compound
Class	Compound classification information
Annot. DeltaMass [ppm]	Detection bias of annotated compounds
Annotation MW	Annotate the Molecular Weight value of the compound theory
Calc. MW	Molecular Weight value of the assay
RT [min]	Retention time
Area	Detected peak area

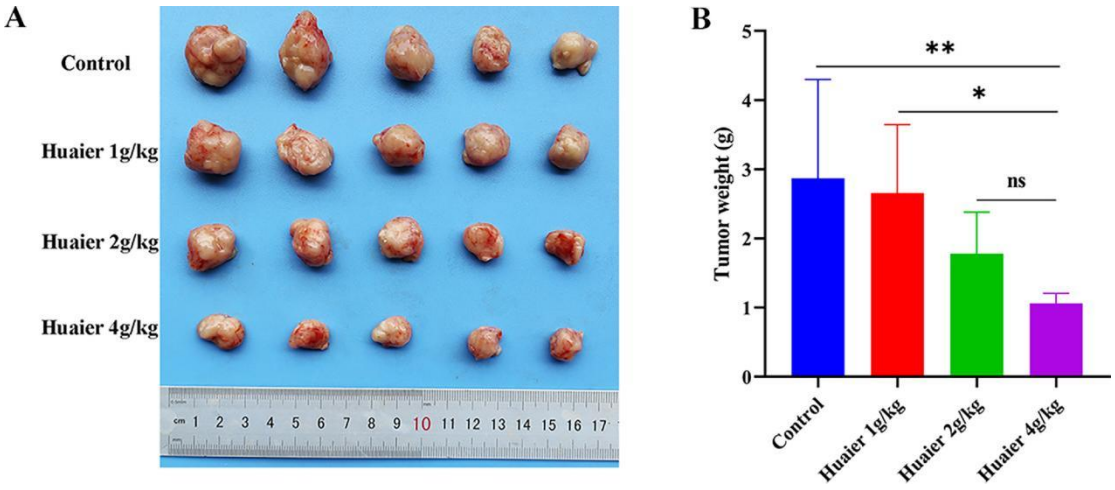

Supplementary Figure 1 The effect of Huaier on the H22-bearing mice. Tumour images (A) and tumor weight (B) of H22-bearing mice after different groups of treatments (n = 5). *P < 0.05 and **P < 0.01 were considered to indicate statistical significance; ns = no significant difference.

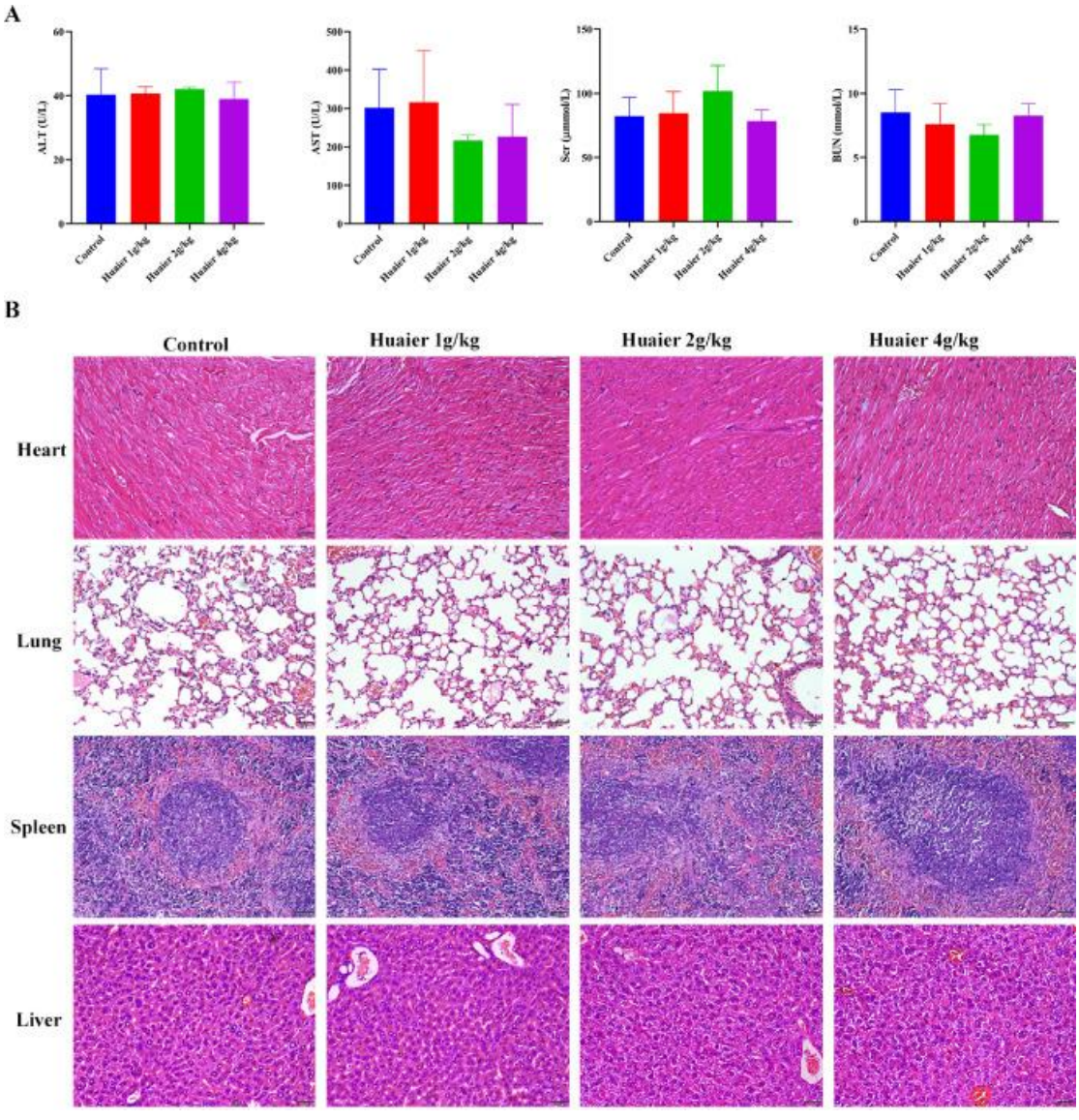

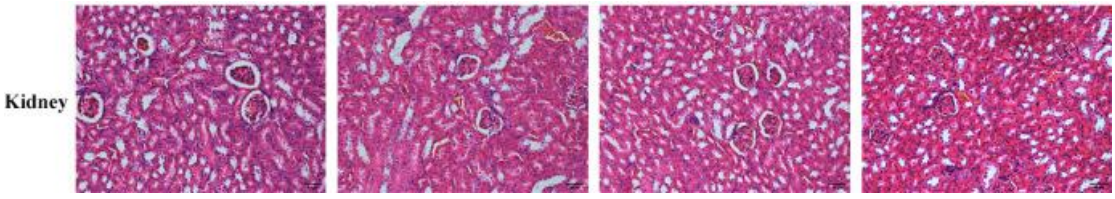

Supplementary Figure 2. The safety evaluation of Huaier on H22-bearing mice. (A) The results of liver and kidney function tests in the experimental mice (n = 3). (B) HE staining of the mice's heart, liver, spleen, lung, and kidney organ pathology sections (×200) (n = 3).

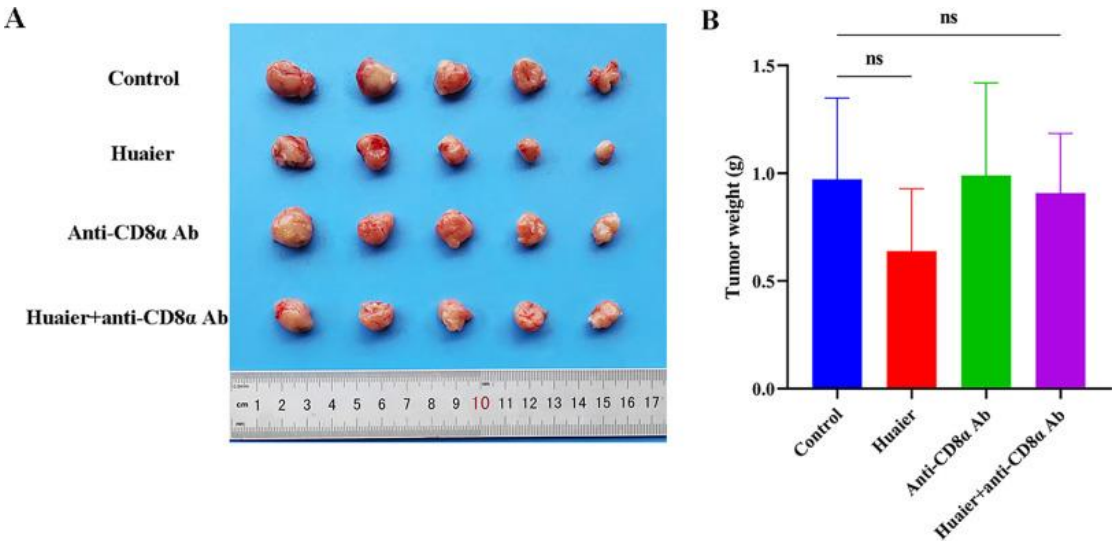

Supplementary Figure 3. The effect of Huaier combined with anti-CD8 α Ab on H22-bearing mice. Tumour images (A) and tumor weight (B) of H22-bearing mice after different groups of treatments (n = 5). ns = no significant difference.

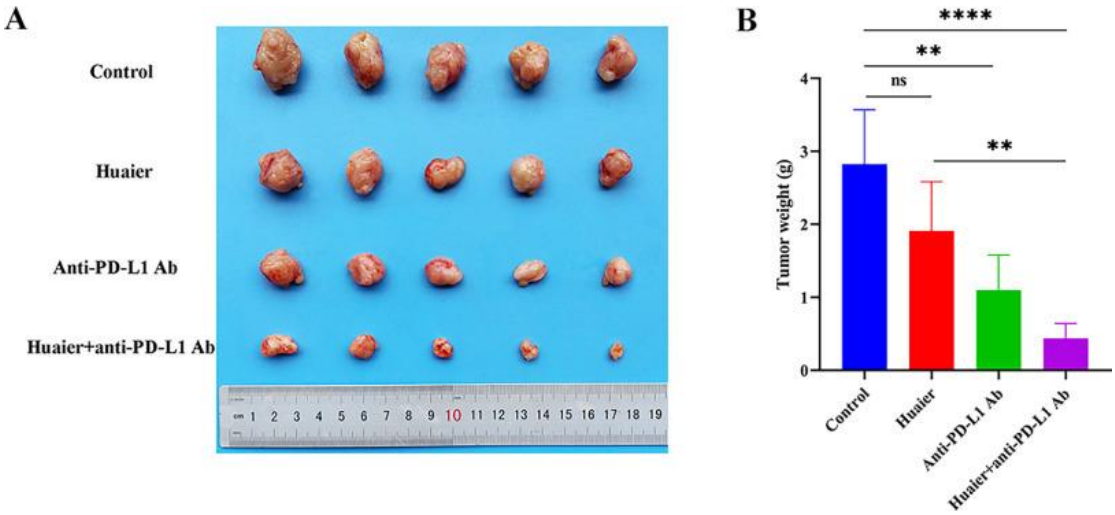

Supplementary Figure 4. The effect of Huaier combined with anti-PD-L1 Ab on H22-bearing mice. Tumour images (A) and tumor weight (B) of H22-bearing mice after different groups of treatments (n = 5). **P < 0.01 and ****P < 0.0001 were considered to indicate statistical significance; ns = no significant difference.

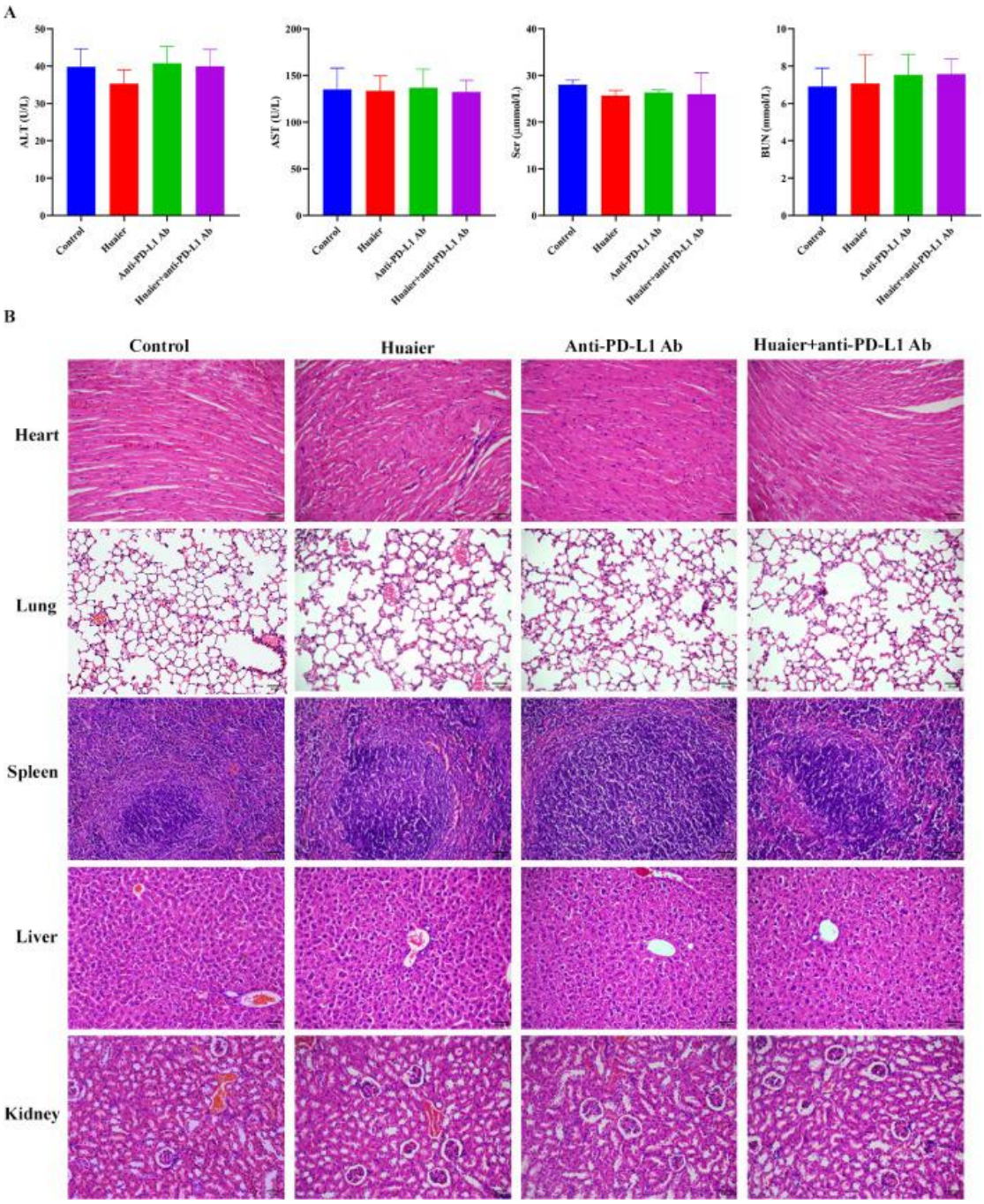

Supplementary Figure 5. The safety evaluation of Huaier combined with anti-PD-L1 Ab on H22-bearing mice. (A) The results of liver and kidney function tests in the experimental mice (n = 3). (B) HE staining of the mice's heart, liver, spleen, lung, and kidney organ pathology sections (×200) (n = 3).